Rewiring *Saccharomyces cerevisiae* metabolism for optimised Taxol® precursors production

Behnaz Nowrouzi [1,2,4,5,6] †, Pablo Torres-Montero [6], Eduard J. Kerkhoven [4,5], José L. Martínez [6], Leonardo Rios-Solis[1,2,3,7*]

[1] Institute for Bioengineering, School of Engineering, The University of Edinburgh, Edinburgh, EH9 3BF United Kingdom

[2] Centre for Engineering Biology, The University of Edinburgh, Edinburgh, EH9 3BD United Kingdom

[3] School of Natural and Environmental Sciences, Molecular Biology and Biotechnology Division, Newcastle University, Newcastle upon Tyne NE1 7RU United Kingdom

[4] Department of Biology and Biological Engineering, Chalmers University of Technology, SE-412 96 Gothenburg, Sweden

[5] Novo Nordisk Foundation Center for Biosustainability, Chalmers University of Technology, SE-412 96 Gothenburg, Sweden

[6] Department of Biotechnology and Biomedicine, Technical University of Denmark, Søltofts Plads Building 223, Kgs. Lyngby, 2800, Denmark

[7] Department of Biochemical Engineering, The Advanced Centre for Biochemical Engineering, University College London, Gower Street, London, WC1E 6BT, UK

Present Address:

† Ingenza Ltd., Roslin Innovation Centre, Roslin, United Kingdom

* Correspondence:

Leonardo Rios-Solis- Leo.rios@ncl.ac.uk

Author Contributions: Behnaz Nowrouzi conceptualised the project and designed and performed the experiments, analysed the data, and wrote the manuscript with input from all

25 authors. Pablo Torres-Montero assisted with bioreactor and HPLC experiments. Eduard J.
26 Kerkhoven, José L. Martínez and Leonardo Rios-Solis coordinated and supervised the study,
27 acquired funding for supporting the study and reviewed the manuscript.

28 **Competing Interest Statement:** The authors declare that the research was conducted in the
29 absence of any commercial or financial relationships that could be construed as a potential
30 conflict of interest.

31 **Abstract**

32 *Saccharomyces cerevisiae* has been recognised as a convenient host for the production of early
33 precursors to the Taxol® anticancer drug. Recent studies have highlighted the harmful impact of
34 oxidative stress as a result of the activity of Taxol® first cytochrome P450-reductase enzymes
35 (*Taxus* spp. CYP725A4-POR). Here, we evolved a new oxidative stress-tolerant yeast strain on
36 galactose, which led to a three-fold higher titre of the CYP725A4 enzyme substrate, taxadiene.
37 We comprehensively analysed the performance of the evolved and parent strain in galactose-
38 limited chemostat cultures before and during oxidative stress induction. Integrating the
39 transcriptomics and metabolite profiling data in an enzyme-constrained genome scale model
40 enabled a more accurate prediction of changes that occurred to biological pathways as a
41 response to/consequence of evolution and oxidative stress. The analyses showed a better
42 performance of the evolved strain with improved respiration and reduced overflow metabolites
43 production. The strain was robust to re-introduction of the oxidative stress, potentially due to the
44 cross-protection mechanism, which contributed to likely better heme, flavin and NADPH
45 availability for an optimal expression of *CYP725A4* and *POR* in yeast. The increased level of
46 taxadiene production has potentially occurred due to the antioxidant properties of taxadiene or as
47 a mechanism to overcome the toxicity of geranylgeranyl diphosphate, the precursor to taxadiene
48 synthase.

49 **Keywords:** *Saccharomyces cerevisiae*, Taxol®, Taxadiene, Oxidative Stress, Adaptive
50 Laboratory Evolution

51 **Acknowledgements and Funding**

57 (FEMS-GO-2021-044), European Molecular Biology Organization Scientific Exchange Grant

58 (9232), British Council - Metabolic Engineering grant (Grant number: R46889), Engineering and

59 Physical Sciences Research Council (Grant number EP/R513209/1) and the Novo Nordisk

60 Fonden, within the framework of the Fermentation Based Biomanufacturing Initiative (Grant

61 number NNF17SA0031362) and the AIM-Bio project (Grant number NNF19SA0057794).

62 **Highlights**

63 - The antioxidant properties of taxadiene promotes its production in *Saccharomyces*
64   *cerevisiae*

65 - *S. cerevisiae* ALE on H_2O_2 and galactose regulates Flavin, iron and NADPH metabolism
66   as well as carbon and protein recycling pathways through cross-protection and
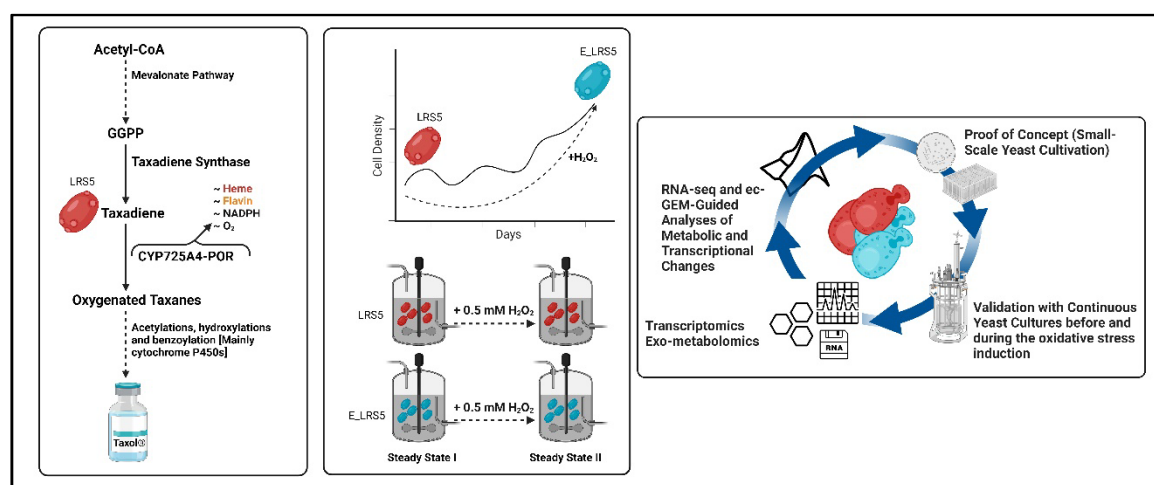67   anticipation mechanisms

68

69

70 Figure 1. **Graphical abstract of the study.** Figure was created with BioRender.com.

71 **1. Introduction**

72 Originally extracted from *Taxus* spp., Taxol® (paclitaxel) is one of the world's best-selling

73 anticancer drugs . While its full biosynthesis pathway has not been elucidated yet, certainly the

74 dominance of cytochrome P450 enzymatic complexes with multiple domains and cofactor

75 requirements including flavins, NADPH and irons (Nowrouzi et al., 2022) has hindered sufficient

76 progress in total drug synthesis by heterologous systems. As a result, the main attention has so

77 far been on optimising the early enzymatic steps. Briefly, Taxol® biosynthesis commences with

78 the conversion of geranylgeranyl diphosphate (GGPP) into the first taxane backbone, taxa-

3

79 4(5),11(12)-diene (taxadiene) and its isomer, taxa-4(20),11(12)-diene (iso-taxadiene), followed by
80 their hydroxylation by the first cytochrome P450, CYP725A4 enzyme, to yield the first
81 diterpenoid/oxygenated taxane, taxadiene-5α-ol (T5α-ol), together with other side diterpenoids
82 (Barton et al., 2016; Edgar et al., 2016; Nowrouzi et al., 2022, Walls et al., 2022b). From there, an
83 array of acetylation, hydroxylation and benzoylation furnishing events lead to Taxol® formation
84 (Lange and Conner, 2021; Walker and Croteau, 2000).
85 We have previously reported on the construction of a high-taxadiene producing *S. cerevisiae*
86 strain, harbouring three copies of taxadiene synthase (*TASY*) genes (Nowrouzi et al., 2020). In a
87 later study, we proposed that the presence of the uncoupling phenomenon potentially fuels the
88 activity of the CYP725A4 enzyme by providing electron and oxygen donors via the radical,
89 reactive intermediates (Nowrouzi et al., 2022). We have also previously shown that increasing the
90 expression of its interacting reductase gene (*POR*) and elevated taxanes concentrations were
91 destructive to the yeast and productivity. This would hinder the use of multiplexing genome
92 editing approaches for increased diterpenoids titre, since the enzymatic-level uncoupling effect
93 would reinforce the oxidative stress (Nowrouzi and Rios-Solis, 2021, Malci et al., 2023). On the
94 other hand, many studies on Taxol® production in *Taxus* spp. displayed a significant impact of
95 biotic and abiotic elicitor application on the terpenoid accumulation (Barrales-Cureño et al., 2022;
96 Escrich et al., 2021; Ketchum et al., 1999; Mirjalili and Linden, 1996). Inspired by this natural
97 phenomenon (Mirjalili and Linden, 1996), we hypothesised that a similar elicitor could potentially
98 stimulate further terpenoid production in yeast. For this reason and to address the associated
99 oxidative stress issue, an adaptive laboratory evolution approach was pursued to adapt the
100 taxadiene-producing yeast cells to increasing concentrations of hydrogen peroxide, with or
101 without dodecane, while growing in galactose-containing complete synthetic mixture to induce the
102 taxanes production in our yeast cells. Using gene expression profiling and exometabolite
103 analysis, we investigated the gene expression profiles of the best-performing evolved colony and
104 the parent strain to examine the alterations in the overall yeast physiology before and during the
105 hydrogen peroxide (H_2O_2) induction in galactose-limited chemostats. We also characterised the
106 associated changes in iron and flavin availability, which were found to be critical to optimal P450-
107 reductase for the next enzyme activity in the Taxol® pathway (CYP725A4-POR) (Nowrouzi et al.,
108 2022). The exometabolite results were also integrated into an enzyme-constrained yeast
109 genome-scale model to interpret the flux changes in each condition with more confidence.
110

111 **2. Materials and Methods**

112

113 ### 2-1. Yeast strains

114 The *S. cerevisiae* strain used for adaptive laboratory evolution was LRS5 (MATa, *leu2-*
115 *3,112::HIS3MX6-pGAL1-ERG19/pGAL10-ERG8;ura3-52::URA3-pGAL1   MvaSA110G/pGAL10-*
116 *MvaE* (codon-optimised)*; his3Δ1::hphMX4-pGAL1-ERG12/pGAL10-IDI1;trp1-289::TRP1_pGAL1-*
117 *CrtE(Xanthophyllomyces   dendrorhous)/pGAL10-ERG20;YPRCdelta15::NatMX-pGAL1-*
118 *CrtE*(codon-optimised)*/pGAL10-CrtE::ARS1014a::pGAL1-TASY-GFP::ARS1622::pGAL1-MBP-*
119 *TASY-ERG20*::ARS1114a::pGAL1-MBP-TASY-ERG20*)*, previously constructed in Nowrouzi et
120 al. study (Nowrouzi et al., 2020)*,* and originated from CEN.PK2-1C (Entian and Kötter, 2007)
121 (EUROSCARF collection). The evolved strain as a result of adaptation to H_2O_2 and galactose
122 was named E_LRS5.

123

124 ### 2-2. Growth media and cultivation platforms

125 The synthetic defined medium (SD) consisted of 0.79 g/L Complete Supplement Mixture (CSM)
126 powder (Formedium), 5 g/L ammonium sulphate (Fisher Chemical™) and 1.7 g/L yeast nitrogen
127 base without amino acids (Thermo Scientific™) and was supplemented with 2% (w/v) galactose
128 (SDG). The routinely used growth medium was composed of yeast extract (1%(w/v)) (Fisher
129 BioReagents™) and casein peptone (2%(w/v)) (Merck), and was supplemented with 2% (w/v)
130 glucose (YPD) or galactose (YPG) (Thermo Scientific™), for inoculum preparation and production
131 screening, respectively. A 20% (v/v) n-dodecane (ACROS Organics™) was used in all
132 cultivations requiring the taxane quantification to extract the taxanes and prevent their air-
133 stripping.

134

135 ### 2-3. EC$_{50}$ determination

136 A fresh LRS5 glycerol stock was streaked on a YPD agar plate and incubated at 30 °C for two
137 days. A 5-mL YPD culture of one randomly picked colony was prepared. Then, one OD_{600} unit of
138 the overnight was inoculated in 2 mL of YPG medium in a 24-well deep well microplate (Axygen)
139 with a variable range of H_2O_2 concentrations to assess the half maximal effective concentration
140 (EC_{50}) of this oxidative stress-inducing agent on taxadiene-producing yeast cell. In a parallel run,
141 YPG medium was further supplemented with 20% (v/v) n-dodecane (ACROS Organics™) to
142 address the same question under both oxidative and phase toxicity stresses, representing a more
143 realistic picture of the oxygenated taxanes-producing cells. The biomass accumulations in both
144 conditions were tested at the end of three days. The EC_{50} values were determined using the
145 dose-response fittings calculated by Origin 2021 software.

146

147 **2-4. Adaptive Laboratory Evolution (ALE)**

148 The same LRS5 glycerol stock was again streaked on a YPD agar plate and incubated at 30 °C

149 for two days. Three independent colonies were then each incubated in 5 mL of YPD liquid

150 medium for one day at 30 °C, 250 rpm. The cells were then inoculated at the starting OD_{600}= 1 in

151 SDG medium using a six-well microplate (Greiner Bio-One™) and were incubated at 30 °C and

152 350 rpm in a thermomixer for 48 hours. The Periodic Challenge/Recovery Scheme methodology

153 proposed by Reyes and Kao (Reyes et al., 2014) was adapted to increase the LRS5 tolerance to

154 increasing concentrations of H_2O_2 (with or without dodecane) while they were producing taxanes.

155 Briefly, one OD_{600} unit of 48-hour cultures were transferred to a 12-well microplate (Greiner Bio-

156 One™) containing new SDG medium. For each colony, an extra technical replicate was also

157 included. Based on the EC_{50} calculations, the cells were initially challenged with 2.13 mM of H_2O_2

158 (H condition) or 0.46 mM of H_2O_2 and 20% (v/v) dodecane (DH condition) for two days and

159 allowed to rest without H_2O_2 presence for the subsequent three days, using 50 µL of inoculum for

160 each cultivation round. During the resting period, for DH condition, dodecane was continued to be

161 supplemented in the fresh medium. Parallel extracellular measurement of H_2O_2 using Pierce™

162 Quantitative Peroxide Assay Kit (Thermo Fisher Scientific) ensured that this compound fully

163 entered the yeast. The cells were routinely cross-checked by microscopy for any microbial

164 contamination. The ALE process (two-day challenge and three-day rest) was repeated until no

165 further improvement in the cell growth was observed, when the final H_2O_2 resistance

166 concentration reached 10 and 12 mM of H_2O_2, with and without dodecane. All colonies were

167 preserved in 50% glycerol at -80 °C for further analysis.

168

169 **2-5. Taxane production assessment of yeast strains**

170 The LRS5 and all evolved strains were incubated in 5 mL of YPD liquid medium at 30 °C, 250

171 rpm. The 24-hr precultures were then inoculated in 1.5 mL of total YPG medium supplemented

172 with 20% (v/v) dodecane in 48-well FlowerPlates (mp2-labs). The plate was sealed with two

173 layers of gas-permeable membrane (Thermo Scientific™) to avoid dodecane evaporation and

174 product loss. The cells were incubated at 30 °C and 800 rpm for 72 hours. By the end of the

175 cultivation, dodecane was extracted from each triplicate set for further analysis with GC-MS and

176 the biomass accumulations were also measured. The best-performing colony, with the highest

177 taxadiene titre, was labelled E_LRS5 and was used for all the subsequent experiments.

178

2-6. Diterpenoid identification and quantification

180 A 50 µL of dodecane overlay was extracted from each culture media and analysed by GC–MS
181 using Trace 1300 GC (ThermoFisher Scientific), equipped with TraceGOLD TG-5MS (30
182 m □×□ 0.25 mm □×□ 0.25 µm). The mass spectra in the range of 40–650 m/z was recorded on a
183 Thermo Scientific ISQ Series single quadrupole mass spectrometer at EI ionisation mode. The
184 GC temperature programme began at 120 °C (three minutes) and was then raised to 250 °C at a
185 rate of 20 °C/minute with a three-minute hold time. Xcalibur™ software (ThermoFisher Scientific)
186 was used to process the data. Geranylgeraniol (GGOH, Sigma Aldrich) was used to quantify the
187 GGOH concentration. The diterpene totarol (Cayman Chemical) was used to quantify the
188 taxanes.

189

2-7. BioLector cultivations for growth rate measurement

191 To determine an appropriate dilution rate for chemostat experiments, BioLector cultivations using
192 a combination of glucose and/or galactose in buffered SD medium (buffered with 0.1 M potassium
193 phthalate monobasic to pH = 6) were performed. The LRS5 and E_LRS5 overnight cultures in
194 YPD were centrifuged at 5000 rpm for 10 minutes, washed with sterile ultrapure water twice, and
195 back diluted to initial OD_{600}= 5 in 1 mL total volume of water. A 30 µL of the cell dilution was then
196 used to inoculate a 48 well flower plate (m2p-labs), containing galactose: glucose ratio of 25, 50,
197 75 and 100 at 1, 2, 3 and 4% total sugar composition. The microplate was sealed with a gas
198 permeable membrane (m2p-labs), and the cultivation was performed in BioLector II
199 microbioreactor at 30 °C and 1000 rpm until the early/full stationary phases were observed for
200 both strains. The maximum specific growth rates for each triplicate were calculated by
201 growthrates R package(Petzoldt, 2020) using a nonparametric smoothing spline function.

202

2-8. Bioreactor cultivations

204 Fresh glycerol stocks of LRS5 and E_LRS5 strains were streaked on new YPD medium for two
205 days. A single colony of each were then grown in 10 mL of YPD medium at 30 °C, 250 rpm and
206 the whole preculture was transferred to 100 mL of buffered SDG medium (pH = 6) in 500-mL
207 baffled shake flasks for additional 1-2 days until a suitable cell density could be achieved for
208 bioreactor inoculation. The preculture cells were then inoculated at initial OD_{600}= 0.1 in triplicates
209 in 1L Biostat Qplus bioreactors (Sartorius Stedim Biotech). The bioreactor cultivations were
210 performed in 500 mL of SDG medium containing 20 g/L galactose (separately autoclaved), 6.7
211 g/L yeast nitrogen base with ammonium sulphate and without amino acids and 0.79 g/L complete
212 synthetic mixture. The pH was adjusted to six using 2 M NaOH, and two drops of antifoam 204

213   (Merck) per liter were added to reduce the foaming. The galactose-limited chemostat cultures

214   started once the off-gas CO_2 started to drop in the batch culture, denoting the depletion of the

215   carbon source. The chemostat cultures were carried out using the same medium supplemented

216   with 10 g/L galactose, at a dilution rate of 0.1 h^{-1}, and it lasted for 50 hours (five residence times)

217   for each steady state. Upon RNA and physiological samplings, the steady state II (SSII) started

218   with the same condition, except that the feeding medium also contained H_2O_2 at a final

219   concentration of 0.5 mM, added separately after the medium was autoclaved. The bioreactors

220   were run at 30 °C with 600 rpm agitation and airflow of 0.5 SPLM. The pH was controlled to

221   remain at six using 2 M of each NaOH and H_2SO_4. The oxygen uptake rate (OUR) and the carbon

222   dioxide evolution rate (CER) values were calculated according to the bioreactor manufacturer's

223   (Sartorius Stedim Biotech) guideline, at 25.4971 L molar volume of gas. The respiratory quotient

224   (RQ) was determined by the following formula:

$$RQ = \frac{CER}{OUR}$$

225

226   **2-9. Dry cell weight and extracellular metabolites measurements**

227   All samplings were performed at the same time after removing the dead volume. The dry cell

228   weights and biomass accumulations during each steady state were measured by retrieving 10 mL

229   of culture broth from each reactor. From that, 1 mL was used for OD_{600} measurement and the

230   other 9 mL were filtered using pre-weighed 0.45-µm MCE filter papers (MontaMil ®). This was

231   followed by drying the filter in the microwave for 10 minutes and 2-3 days of desiccation. The

232   extracellular metabolites including ethanol, succinate, acetate, glycerol and pyruvate productions

233   of both steady states and strains were analysed using ion-exchange HPLC. The samples were

234   first filtered using a 0.45 µm filter. The samples were then analysed by injecting them into a Bio-

235   Rad Aminex HPX-87H column at 60 °C. The injection volume was 20 µL and the elution solvent

236   was 5 mM H_2SO_4 at a flow rate of 0.6 mL min^{-1}. The off-gas ethanol was also included in the

237   total ethanol flux measurement.

238

239   **2-10. Statistical analyses for biomass and flux measurements**

240   All statistical analyses of this study were performed in R version 4.1.3. Two-way analysis of

241   variance (ANOVA) was used to study the effect of the strain type and the continuous culture state

242   (steady states I or II) on carbon recovery and flux changes, using R stats package. The

243   Bonferroni-corrected t-test was performed for the pairwise comparisons, at a significance of

244   adjusted $p < 0.05$. The biomass and taxanes production by the evolved and parent cells were

245   compared using the Kruskal-Wallis test. For the same analysis, the pairwise comparison against

246 the control condition was performed by Dunnett's multiple comparisons test at a significance of p

247 < 0.05, using DescTools R package (Signorell et al., 2022).

248

249 **2-11.** **Sampling for transcriptomics analysis**

250 The RNA-seq samplings were performed by discarding the dead volume followed by retrieving 1-

251 mL culture broth at a minimum of 10 OD_{600} units in Eppendorf tubes, which were pre-cooled at -

252 20 °C. The samples were immediately placed on ice and quickly centrifuged in a pre-chilled

253 centrifuge for two minutes at 19,341 ×g. Upon removing the supernatants, the samples were flash

254 frozen in liquid nitrogen and stored at -80 °C for further analysis.

255

256 **2-12.** **Total RNA extraction and Library preparation with polyA selection and**

257 **HiSeq sequencing**

258 Total RNA was extracted using Qiagen RNeasy Plus mini kit following the manufacturer's

259 instructions (Qiagen). Extracted RNA samples were quantified using Qubit 2.0 Fluorometer (Life

260 Technologies) and RNA integrity was checked using Agilent TapeStation 4200 (Agilent

261 Technologies). RNA sequencing libraries were prepared using the NEBNext Ultra II RNA Library

262 Prep Kit for Illumina following the manufacturer's instructions (NEB). Briefly, mRNAs were first

263 enriched with Oligo(dT) beads. Enriched mRNAs were fragmented for 15 minutes at 94 °C. First

264 strand and second strand complementary DNAs (cDNAs) were subsequently synthesised. The

265 cDNA fragments were end repaired and adenylated at 3'-ends, and universal adapters were

266 ligated to cDNA fragments, followed by index addition and library enrichment by limited-cycle

267 PCR. The sequencing libraries were validated on the Agilent TapeStation (Agilent Technologies)

268 and quantified using Qubit 2.0 Fluorometer (Invitrogen) as well as by quantitative PCR (KAPA

269 Biosystems) (Figure S3. 1 and Table S3. 1). The sequencing libraries were clustered on a flowcell

270 lane. After clustering, the flowcell was loaded on the Illumina HiSeq instrument (4000 or

271 equivalent) according to the manufacturer's instructions. The samples were sequenced using a

272 2x150bp Paired End (PE) configuration. Image analysis and base calling were conducted by the

273 HiSeq Control Software. Raw sequence data (.bcl files) generated from Illumina HiSeq was

274 converted into fastq files and demultiplexed using Illumina's bcl2fastq 2.17 software. One

275 mismatch was allowed for index sequence identification.

276

277 **2-13.** **RNA-seq analysis**

278 RNA-seq data was processed using nf-core RNA-seq pipeline version 3.7 (Ewels et al., 2020),

279 run on Nextflow version 20.12.0-edge and singularity configuration profile (Di Tommaso et al.,

280   2017). After pre-processing the reads, they were mapped onto reference Ensembl yeast R64-1-1

281   genome (available on Amazon Web Services iGenomes) by Salmon (Patro et al., 2017), followed

282   by transcript abundance quantification using the same software with the default parameters. The

283   data quality was checked with multiQC software (Ewels et al., 2016). The tximport R package

284   (Soneson et al., 2015) was then used to aggregate the transcript-level estimates into gene level

285   abundances before differential gene expression using the Wald test implemented in the DESeq2

286   R package (Love et al., 2014) for both effect-based and pairwise comparisons. The lfcShrink

287   function with ashr shrinkage estimator (Stephens, 2017) was then used to estimate the

288   expression changes more accurately. The differentially expressed genes were filtered by an

289   adjusted p value of < 0.05 and log2 fold change threshold at zero. The pathway enrichment

290   analyses were performed with pathfindR (Ulgen et al., 2019) R package, based on the Kyoto

291   Encyclopedia of Genes and Genomes (KEGG) database (Kanehisa and Goto, 2000) and the p

292   values were adjusted using the default Bonferroni method. The package org.Sc.sgd.db (Carlson,

293   2019) was used for gene ontology (GO) overrepresentation analysis using clusterProfiler (Yu et

294   al., 2012) package, with p values corrected according to Benjamini and Hochberg's false

295   discovery rate test (Benjamini and Hochberg, 1995). The gene sets smaller than 10 and larger

296   than 500 genes were ignored for both GO and KEGG enrichment analyses. All RNA-seq

297   analyses were performed on Eddie, The University of Edinburgh's high-performance computing

298   cluster using 12 cores of 10 Gigabytes RAM memory in Intel® Xeon® Processor E5-2630 v3 (2.4

299   GHz) processor.

300

301   **2-14.   Preparation of models and flux balance analysis**

302   The ecYeastGEM model (GECKO toolbox 2.0 (Domenzain et al., 2022);

303   ecYeastGEM_batch.mat) was used as the yeast model. This enzyme-constrained model already

304   contained 8028 reactions and 4153 metabolites and was manipulated by adding 32 reactions and

305   24 metabolites with separate forward and reverse, arm and protein exchange reactions for

306   terpenes synthesis and their import and export, to achieve mass balance. For both strains under

307   the stress, the models were extended with hydrogen peroxide intracellular transport and

308   exchange reactions to resemble the stress condition. The coefficients of the enzyme

309   pseudometabolites in each reaction were calculated according to Sánchez et al. (Sánchez et al.,

310   2017), by querying the K_{cat} values from BRENDA database (Chang et al., 2021). When the Kcat

311   values were not directly available for the enzymes, it was calculated using the following formula:

312
$$Kcat\left(\frac{1}{h}\right) = \frac{SA\left(\frac{\frac{\mu mol}{mg}}{min}\right) \times MW\left(\frac{g}{mol}\right) \times 60\left(\frac{min}{h}\right) \times 10^3\left(\frac{mg}{g}\right)}{10^6\left(\frac{\mu mol}{mol}\right)}$$

313

314   where SA is the specific activity and MW is the molecular weight of the enzyme. The heterologous
315   genes in the mevalonate (MVA) pathway were added to their associated reactions in the model.
316   The script for addition of the new reactions and related modifications is available in the figshare
317   repository: https://figshare.com/s/3f00d32c57c2a189d2db;DOI: 10.6084/m9.figshare.20424801.

318

319   Four models, two per strain (for each steady state), were then created by constraining the fluxes
320   of off-gas and exo-metabolomes at a fixed growth rate (dilution rate), considering 5%
321   measurement error to avoid model over-constraining. The reactions related to medium
322   components uptakes, terpene export, unmeasured metabolic fluxes and overflow metabolites
323   were set to open with a maximum upper boundary (UB) of 1000 and lower boundary (LB) of -
324   1000 mmol/gDW/h. The models were then optimised by FBA by setting the non-growth
325   associated maintenance (NGAM) reaction (r_4046) as the objective function. After fixing the
326   NGAM reaction boundaries by the calculated value from the FBA analysis, the flux through
327   cytoplasmic, mitochondrial and peroxisomal thioredoxin reactions (r_0550No1; r_0550No2;
328   r_0551No1; r_0552No1; r_0552No2) were set open to activate the core antioxidant mechanism in
329   all models. The manipulation of the models was finalised by minimising the total enzyme pseudo-
330   metabolite pool exchange flux. All simulations were performed using COBRA Toolbox (Heirendt
331   et al., 2019; Schellenberger et al., 2011) with Gurobi Optimiser (version 9.5.1) as the solver in
332   MATLAB R2021a.

333

334   **2-15.   Random sampling of the solution spaces and flux enrichment analysis**
335   The random sampling algorithm implemented in RAVEN toolbox (Agren et al., 2013; Wang et al.,
336   2018) was employed to investigate the flux distributions in each enzyme-constrained model. A
337   total of 10,000 random samples were collected for each model followed by their pairwise
338   comparisons by the Kruskal-Wallis test. Upon normalizing the results by the average CO_2
339   production flux value, COBRA Toolbox (Heirendt et al., 2019; Schellenberger et al., 2011) flux
340   enrichment analysis function was used to perform pairwise comparisons of means of random
341   samples from each model to find the changes in fluxes through enrichment by their genes, using
342   hypergeometric 1-sided test and false discovery rate (FDR) correction for multiple testing at a
343   significance level of 0.05 and fold change cut-off = 1. The intersection of the genes enriched by
344   gene expression and flux enrichment in the same regulation direction showed the flux-gene
345   expression correlations. The whole random sampling analysis was performed in MATLAB
346   R2021a on VLX servers on XRDP Linux Remote Desktop, hosted by the School of Engineering at
347   The University of Edinburgh.

348

349

3. Results & Discussion

351

3-1. Evolving taxadiene-producing yeast on H_2O_2 as an elicitor for higher Taxol® precursors production

Earlier we reported that the higher oxygenated taxanes production by *Taxus cuspidata* CYP725A4 and POR was associated with the release of reactive metabolites, potentially acting as oxygen/electron donors while imposing oxidative stress on yeast (Nowrouzi et al., 2022). Therefore, a robust yeast cell factory for producing highly oxygenated taxanes like Taxol® was needed to efficiently address this paradoxical issue. To further examine if the oxidative stress and overall, the toxicity issue, was related to oxygenated-taxanes production, our preliminary experiments tested the effect of increasing concentrations of hydrogen peroxide (H_2O_2), a known oxidant agent, on several of our in-house yeast strains. These included the wild-type CEN.PK strain, an engineered CEN.PK strain with overexpressed genes in mevalonate (MVA) pathway (mGTy116) (Reider Apel et al., 2017), taxadiene-producing mGTy116 (LRS5) (Nowrouzi et al., 2020) and oxygenated taxanes-producing LRS5 (LRS6) (Walls et al., 2020) in YPG medium supplemented with dodecane, representing a realistic, normal scenario, under which taxanes are induced and removed *in situ* by an organic overlay. The results revealed the superiority of LRS5 in final biomass compared to mGTy116 and LRS6, where almost half of LRS5 final biomass was retained at 2 mM final H_2O_2 concentration (Figure 2A). Hence, we initially concluded that the LRS5 strain might resist the oxidative stress, while mGTy116 showed the weakest resistance, likely due to overaccumulation of toxic prenyl pyrophosphates (Martin et al., 2003). This observation further strengthened our hypothesis that adapting LRS5 to increased oxidative stress would benefit the biomass and taxadiene production over time, as we earlier showed a strong correlation between the biomass accumulation and taxadiene production by LRS5 (Nowrouzi et al., 2020).
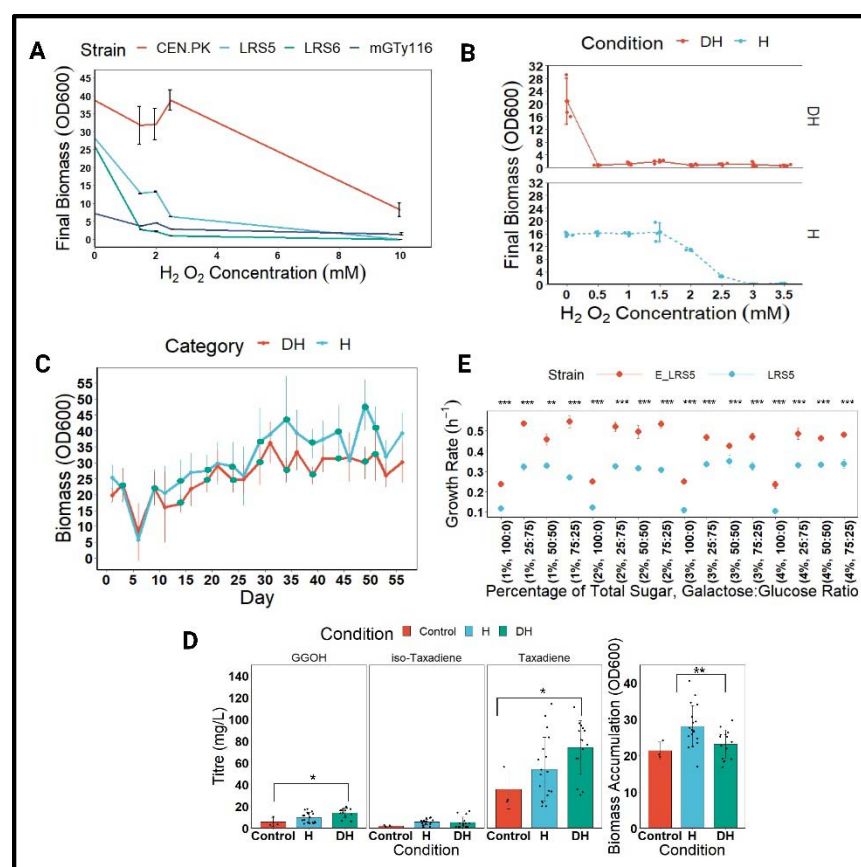
375

376

Figure 2. **Summary of adaptive laboratory evolution results and small-scale physiological parameters measurements.** A) The effect of increased concentration of H_2O_2 on the final biomass of selected yeast strains. All strains were cultivated in YPG+20% (v/v) dodecane medium for three days at 30 °C, 450 rpm. CEN.PK: CEN.PK2-1C (Entian and Kötter, 2007); mGTy116: CEN.PK yeast strain with overexpressed genes in mevalonate pathway (Reider Apel et al., 2017); LRS5: mGTy116 harbouring three copies of taxadiene synthase genes (Nowrouzi et al., 2020); LRS6: LRS5 harbouring *Taxus cuspidata* taxadien-5α-hydroxylase (*CYP725A4*), cytochrome P450 reductase (*POR*) and taxa-4(20),11(12)-dien-5α-olO-acetyl transferase (*TAT*) genes for production of oxygenated and acetylated taxanes (Walls et al., 2020). The data show the mean ± SD of biological triplicates. B) EC_{50} determination for LRS5 under dodecane and hydrogen peroxide (DH) or hydrogen peroxide (H) stresses. The LRS5 strain was cultivated for three days at 30 °C, 450 rpm. For all DH conditions, 100% dodecane was utilised. The data show the mean ± SD of biological triplicates. C) Biomass plot for adapting the taxadiene-producing strain (LRS5) to H_2O_2 (H) and H_2O_2+Dodecane (DH), while growing on a complete synthetic mixture with 2% (w/v) galactose (SDG). The line plots represent the mean ± SD of three biological and two technical replicates. The green dots on each plot show the start of the H_2O_2 induction period. The increasing H_2O_2 concentrations (concentration increased every 5 days) at H condition were: 2.13, 2.13, 2.63, 3.63, 4.63, 6, 8, 10, 10, 12 and 12 mM. The increasing H_2O_2 concentrations at DH condition (increased concentration every 5 days and then fixed) were:

13

394   0.46, 0.46, 1, 2, 2, 3, 5, 8, 10, 10 and 10 mM. The values were selected based on the biomass results

395   obtained at the end of each resting period. D) Taxanes and biomass accumulation from parent strain

396   (control: LRS5) and evolved strains (E_LRS5 from H (H_2O_2) and DH (H_2O_2+Dodecane) conditions) after 72-

397   hour cultivations in YP-galactose medium (2% w/v) at 30 °C. The data show mean ± SD of three biological

398   and two technical replicates for the evolved strains and triplicates of the parent strain (LRS5). The asterisks

399   indicate significant differences by Dunnett's multiple comparisons test (***: adjusted $p < 0.001$, **: adjusted p

400   < 0.01, *: adjusted $p < 0.05$), relative to control conditions (SS II vs. SSI and/or E_LRS5 vs. LRS5). E)

401   Growth rates comparison of the best-performing evolved colony (E_LRS5) and parent strain (LRS5) in SDG

402   medium (pH = 6) containing 1-4% total sugar at 25-100% galactose: glucose ratios. The mean ± SD values

403   of biological triplicates are shown. Figure was created with BioRender.com.

404

405   Biphasic culture systems tend to reduce the toxicity and air-stripping of terpenoids produced by

406   the microbial cells (Ajikumar et al., 2010; Nowrouzi et al., 2020; Sarrade-Loucheur et al., 2020).

407   However, the used organic overlay might inevitably be toxic (Jongedijk et al., 2015; Santoyo-

408   Garcia et al., 2022, Galindo-Rodriguez et al., 2023, Santoyo-Garcia et al., 2023). Therefore, to

409   address the oxidative stress with or without the potential overlay phase toxicity under the

410   continuous production of terpenes, two evolution lines were designed to increase the resistance

411   towards the hydrogen peroxide (H) or dodecane and hydrogen peroxide (DH), starting with a

412   suitable dose of H_2O_2 in which at least 50% final biomass could be preserved (EC_{50}) (Figure 2B).

413   By the end of 56 days, the H_2O_2 concentration tolerance was increased by 5.6-fold and 21.9-fold,

414   at H and DH conditions, respectively (Figure 2C).

415   As illustrated in Figure 2D, the initial screening of the evolved and the parent strain revealed that

416   the taxadiene and its isomer, iso-taxadiene, and geranylgeraniol (GGOH), the dephosphorylated

417   by-product of taxadiene synthase substrate (geranylgeranyl diphosphate; GGPP) (Song et al.,

418   2017), were all increased by 2.3-, 2.5-, and 2.4-fold, and 2.1-,1.5-, and 1.6-fold, in DH and H

419   conditions, respectively, with taxadiene and GGOH production being significantly higher in DH

420   condition compared to the control ($p = 0.045$ and $p = 0.012$). The final biomass from both H and

421   DH were found to be significantly different from each other ($p = 0.008$), but remained relatively

422   similar to that of control. While we achieved superior product titre in DH condition, potentially due

423   to the strains' pre-adaptation to dodecane or the dodecane acting as an oxygen vector (Blaga et

424   al., 2018), for the sake of simplicity in our study design, the rest of our study only focused on the

425   H condition. Here, we solely further investigated the performance of the best-performing colony

426   evolved from the H condition which we called E_LRS5. The overall taxadiene, iso-taxadiene and

427   GGOH titres by E_LRS5 were 103.3 ± 15.2, 4.00 ± 3.4 and 11.8 ± 2.3 mg/L, which represented a

428 2.9- (adjusted p = 0.005), 1.7- (adjusted p = 0.001), and 3.3-fold (adjusted p = 0.001)

429 improvement compared to the original LRS5. Similarly, the final biomass accumulation of

430 E_LRS5 also improved by around 1.6-fold to 33.3 ± 3.9 (adjusted p = 0.011), representing a two-

431 fold improvement in the taxadiene yield (3.1 mg/L/OD_{600}). All associated chromatograms and

432 mass spectra are provided in Figures S1-3.

433 To mimic the oxidative stress induction under the controlled conditions, we then sought to study

434 the E_LRS5 and LRS5 physiologies in chemostat cultures, for which we first attempted to

435 determine a dilution rate suitable to both strains. Due to the slow growth of *S. cerevisiae* on

436 galactose compared to glucose (Paulo et al., 2015), the effect of different galactose: glucose

437 composition at 1 to 4% final total sugar concentration was investigated in BioLector

438 microbioreactors using complete synthetic mixture media without any dodecane addition. The

439 results showed that the growth rate significantly increased in all cases in comparison to the LRS5

440 strain (Figure 2E). Our results were however contrary to Hong et al. study (Hong and Nielsen,

441 2013), where the maximum specific growth rate of the galactose-adapted yeast strains was lower

442 in a glucose medium. In our study, the maximum growth rate at 3% galactose condition for

443 E_LRS5 (0.25 ± 0.01) exceeded by around 1.6-fold from the maximum specific growth rate of

444 0.16 h^{-1} reported for CEN.PK 113-7D during the aerobic batch cultivation in a 3% galactose-

445 containing medium (de Jongh et al., 2008). As illustrated in Figures S4-5, notably, the lag phase

446 in the evolved strain using pure galactose was also longer by approximately two-fold with a

447 shorter exponential phase, potentially as a protection mechanism against the stress (Kussell,

448 2013).

449

450 **3-2. Respiration is an antioxidant defence mechanism in H_2O_2 and galactose-evolved**

451   **taxadiene-producing yeast**

452 Maximum growth rates (μ_{max}) of 0.12 ± 0.01 for LRS5 and 0.24 ± 0.01 h^{-1} for E_LRS5 were

453 achieved under 1% galactose addition, therefore our subsequent chemostat experiments were

454 performed at a dilution rate of 0.1 h^{-1}. This also presented us with the advantage of eliminating

455 the negative catabolite repression effect of glucose on the induction of galactose promoters,

456 which we previously used to overexpress several of the MVA pathway as well as the taxadiene

457 synthase genes in LRS5 (Nowrouzi et al., 2020), while we appreciate that depending on the

458 strain, the galactose: glucose ratio sensing can play a role in GAL genes induction (Renan et al.,

459 2015). To mimic the stress associated with oxygenated taxanes products in yeast, the LRS5 and

460 E_LRS5 physiologies were studied through RNA-seq, off-gas and exo-metabolites analyses

15

461   before (steady state I; SSI) and during the oxidative stress induction (steady state II; SSII) in
462   chemostats. To study the impact of evolution and oxidative stress, besides the differential gene
463   expression analysis, enrichment analysis with respect to protein-protein interaction subnetworks
464   (Ulgen et al., 2019) were performed (Tables S2-4; Figures S6. D-E). To this end, at cut-off of log2
465   fold change (LFC) = 0 and FDR < 0.05, 1607 and 1675 genes were found to be up- and
466   downregulated, respectively, by the evolution (Figure S6. B), from which 90% and 73% were
467   uniquely up- and downregulated, respectively, highlighting the significant impact of adaptive
468   laboratory evolution on the overall superior performance of E_LRS5. This was further supported
469   by the clear genotype separation by principal component analysis (PCA) (Figure S6. A). The
470   number of upregulated and downregulated genes remarkably decreased to 176 and 455, and 223
471   and 106 for oxidative stress and interaction factors, respectively, denoting the relative robustness
472   of E_LRS5 against oxidative stress.

473   To investigate the metabolic mechanisms underlying the different physiologies of both strains
474   under the two steady states, an enzyme-constrained yeast genome scale model was used to
475   generate condition-specific models, followed by optimisation towards the maximisation of ATP
476   production (non-growth associated maintenance (NGAM)) and unconstraining the thioredoxin-
477   using reactions, as the heterologous protein production/H_2O_2 induction is correlated with
478   increased antioxidant defence mechanism in yeast (Garrido and Grant, 2002). This was followed
479   by random sampling to study the metabolic fluxes with respect to evolution and oxidative stress
480   induction to identify the up- and down-regulated reactions (E_LRS5 vs. LRS5 and their
481   corresponding steady states) at cut-off = 1 and FDR < 0.05, based on the statistically significant
482   overrepresented genes from the flux enrichment analysis (McGarrity et al., 2020).

483   The carbon recovery profiles revealed that the major contributor to the overflow metabolites was
484   ethanol (SSI-SSII, LRS5: 23.3 ± 1.90 % and 25 ± 0.61 %, E_LRS5: 16.5 ± 1.21 % and 17.4 ±
485   1.32 %), followed by acetate at a minor level (SSI-SSII, LRS5: 6.64 ± 0.25 % and 7.25± 0.35 %,
486   E_LRS5: 6.72 ± 0.86 % and 7.66 ± 0.58 %) (Figure 3A); During SSI, E_LRS5 produced less
487   ethanol, acetate, CO_2 and glycerol, in contrast to pyruvate (Table S1). However, this reduction
488   was only significant for ethanol (adjusted p = 0.00016), glycerol (adjusted p = 3.057e-05) and
489   pyruvate (adjusted p = 1.4e-06) production. Succinate production remained negligible for LRS5,
490   while we did not detect this compound in the E_LRS5 medium. The pyruvate dehydrogenase
491   bypass, composed of pyruvate decarboxylase (PDH), aldehyde dehydrogenase (ADHs) and
492   acetyl-CoA synthase (ACSs), plays an intermediate role in the production of the major source of
493   cytoplasmic acetyl-CoA in yeast (Qin et al., 2020) while decarboxylating the pyruvate to ethanol
494   and acetate, also producing NADPH. The higher accumulation of pyruvate in E_LRS5 SSI culture

495   associates well with the downregulation of the genes of pyruvate-catabolising PDC1, PDC5 and

496   DLD1, and the upregulation of pyruvate-synthesising *PYK2* and *AGX1* (McNeil et al., 1994). The

497   lowered acetate flux is probably due to the downregulation of the mitochondrial *ALD5* and

498   cytosolic *ALD6* and their catalysing reactions. Despite this, we observed the downregulation of

499   acetate-using *ACS1* and *ACS2*, where it is likely that the upregulation in *LAT1* and *LPD1*

500   expressions together with others like mitochondrial acetyl-CoA transferase *ACH1* effectively

501   replaced ACSs to produce the acetyl-CoA. At the same time, the absence of succinate in

502   E_LRS5 cultures relates to the general upregulation of succinate dehydrogenases (*SDH1*, *SDH2*,

503   *SDH3* and *SDH4*), which compensated for the slight upregulation of succinate-consuming *LSC2*.

504   While the lower ethanol exchange flux cannot be explained by the upregulation of *ADH3* and

505   *ADH4* and their predicted reaction fluxes and the downregulation of ethanol-metabolising *ADH2*,

506   we can postulate the lowered reaction fluxes from pyruvate consumption mainly be due to

507   decreased flux through pyruvate decarboxylation reactions. The downregulation of glycerol-

508   producing *GPD2* and *GPP1* as well as dihydroxyacetone phosphate-accumulating *GUT2* and

509   *DAK2*, and upregulation of glycerol-consuming *GPD1*, *GPP2* and *GUT1*, justify the reduced

510   glycerol production by E_LRS5.
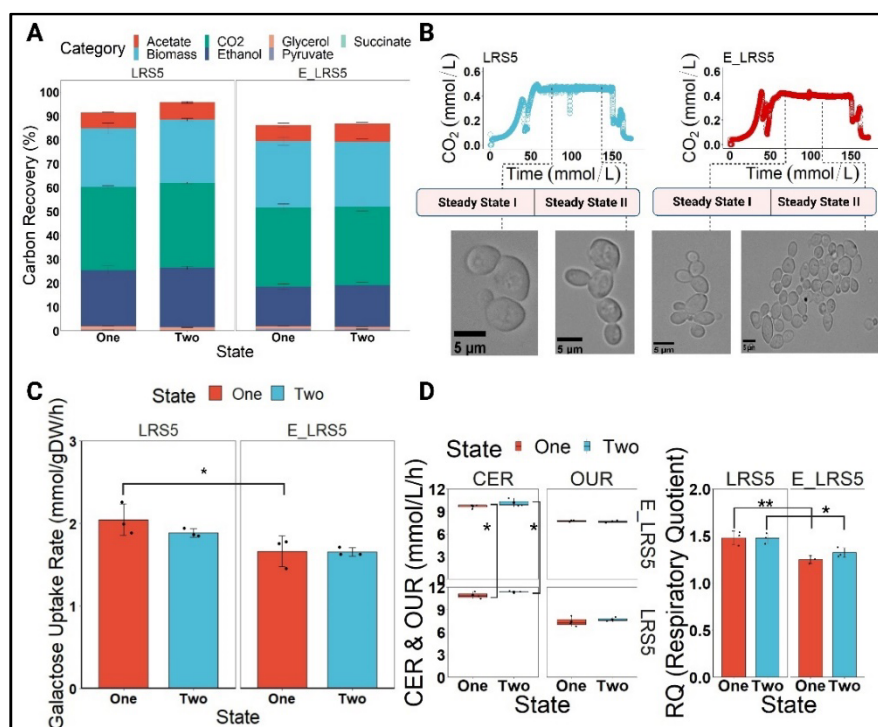
511

512   Figure 3. **Phenotyping.** A) Total carbon recovery for LRS5 and E_LRS5, normalised per mmol of galactose

513   for ethanol, acetate, glycerol, pyruvate, and succinate. The mean ± SD of biological triplicates is shown. The

514   summary of only statistically significant adjusted p values from the t-test (threshold: adjusted p < 0.05) for
515   comparison of product-based carbon recovery is as follows: Glycerol (LRS5: One-E_LRS5: One: 0.0003;
516   E_LRS5: Two-LRS5: Two: 0.009); Ethanol (LRS5: One-E_LRS5: One: 0.001; LRS5: Two-E_LRS5: Two:
517   0.001); Pyruvate (LRS5: One-E_LRS5: One: 2.22e-07; LRS5: Two-E_LRS5: Two: 6.55e-08). B) Microscopic
518   images of LRS5 and E_LRS5 in continuous cultures before and during oxidative stress induction. The bars
519   represent 5 μm and the images were taken under 100X magnification using a Motic BA310E microscope
520   (Motic, Hong Kong). C) Galactose uptake rates by LRS5 and E_LRS5 chemostat cultures. The cells were
521   cultivated in SDG medium, containing 10 g/L galactose, at a dilution rate of 0.1 h^{-1}, during steady state I
522   (SSI), without extra oxidative stress, and with 0.5 mM H_2O_2 continuously feeding the cell *(steady state II;*
523   *SSII).* The data show mean ± SD of triplicates. D) OUR, CER and RQ plots for LRS5 and E_LRS5. The data
524   show the mean ± SD of biological triplicates. The asterisks indicate significant differences by pairwise t-test
525   (***: adjusted p < 0.001, **: adjusted p < 0.01, *: adjusted p < 0.05), relative to control conditions (SS II vs.
526   SSI and/or E_LRS5 vs. LRS5). Figure was created with BioRender.com.

527   Upon introduction of the oxidative stress agent, the ethanol and acetate production fluxes further
528   increased, which might be due to the strong downregulation of *ADH2*. It is known that the higher
529   biomass yield can lead to a higher acetate production (Ostergaard et al., 2000), which was in
530   accordance with the higher acetate flux in E_LRS5 upon oxidative induction. Furthermore, the
531   upregulation of *ACS2* and its catalysing reaction flux at E_LRS5 SSII explains the higher
532   accumulation of acetate, similar to LRS5. Compared to LRS5, the E_LRS5 also showed 1.3- and
533   1.2-fold higher biomass yields per mmol of consumed galactose at SSI (adjusted p = 0.007) and
534   SSII (adjusted p = 0.038), respectively, depicting the better carbon usage in this strain compared
535   to the parent strain (Table S1). An increased TCA capacity can reduce the carbon conversion to
536   ethanol and NADH oxidation into glycerol (Vemuri et al., 2007), explaining the lower glycerol and
537   ethanol accumulation by E_LRS5.

538   **3-3. Anticipation and cross-protection mechanisms act to promote the carbon and**
539   **protein recycling pathways upon oxidative stress re-induction, in H_2O_2 and**
540   **galactose-adapted taxadiene-producing yeast**
541   We noticed a remarkable difference in the yeast morphology between both strains (Figure 3B),
542   where the yeast cells showed more budding scars in the E_LRS5 culture compared to LRS5, and
543   this improved further upon the oxidative stress induction, although similar dry cell weights for
544   E_LRS5 strain were obtained at both steady states (SSI: 2.43 ± 0.15 g/L and SSII: 2.39 ± 0.11
545   g/L) which might be due to the reduction in cell volume and mitochondrial network expansion
546   (Kim et al., 2020).

547   Earlier we reported on the filamentous growth of LRS5 due to nutrient starvation (Walls et al.,
548   2022). While we did not observe such elongated filamentous phenotype in our study, one can first
549   relate such morphology to non-quiescence, with characteristics including impaired mitochondrial
550   respiration, decreased trehalose and glycogen conservation and life span extension by chronic
551   oxidative stress (Mohammad et al., 2020). In comparison, however, E_LRS5 depicted a higher
552   respiratory capacity with a 1.2-fold lower RQ value (1.25 ± 0.04 vs. 1.48 ± 0.07; adjusted p =
553   0.004) (Figure 3D), with similar values at SSII, 1.48 ± 0.06 (LRS5) and 1.32 ± 0.05 (E_LRS5)
554   (adjusted p = 0.039), justifying the lower ethanol accumulation by E_LRS5. We also observed the
555   upregulation of trehalose and glycogen biosynthesis (*GLC3*, *GSY1*, *GPH1*) and downregulation of
556   glycogen hydrolysis, glucoamylases and glucanases like *EXG1*, *BGL2* and β-1,3-glucan synthase
557   *FKS1*. Similarly, *NCW2*, a deletion of which is known to activate the glucan and chitin
558   biosynthesis in the yeast cell wall, was amongst the most strongly downregulated genes (LFC: -
559   2.18) (Queiroz et al., 2020), which interestingly became the most strongly upregulated gene
560   considering the evolution and oxidative stress interaction effect (LFC: 0.69). Similarly, we noticed
561   the general downregulation of the Leloir pathway genes and regulators and reaction fluxes
562   (*GAL1*, *GAL2*, *GAL3*, *GAL7*, *GAL10*, *GAL11* and *GAL80*), which was in accordance with 1.2-fold
563   lower galactose consumption rate in E_LRS5 (1.66 ± 0.2 mmol/gDW/h; adjusted p = 0.038), with
564   almost similar value achieved at SSII (1.65 ± 0.05 mmol/gDW/h) (Figure 3C). The upregulation of
565   *PGM2*, with the enzyme at the glycolysis and pentose phosphate pathway (PPP) branches, was
566   also in line with Hong and Nielsen (Hong and Nielsen, 2013) study, where the adaptive laboratory
567   evolution on galactose resulted in overexpression of *PGM2* towards the trehalose and glycogen
568   biosynthesis. We concurrently observed a strong significant upregulation in maltases like *MAL12*,
569   *MAL32*, isomaltase *IMA1*, glucose-producing glycogen phosphorylase *GPH1* and most hexose
570   transporters (*HXT17*, *HXT6*, *HXT13* and *HXT7*). Considering both evolution and oxidative stress,
571   however, the *HXT6* gene was downregulated, without any other changes in the other stated
572   genes. Hence, we can postulate that to combat the carbon starvation at the next oxidative stress
573   induction, E_LRS5 preferentially invested in recycling the intracellular carbon instead of taking up
574   more galactose and for this, it tended to synthesise the long-chain carbons as protecting and
575   carbon-storing agents (Kocaefe-Özşen et al., 2022). Further to this hypothesis, except the
576   upregulation of *TDH2*, *PGK1*, *PGM2*, *GPM1*, *GPM3* and *PYK2*, we observed the downregulation
577   of glycolysis pathway genes, and the reaction fluxes, as well as the upregulation of non-oxidative
578   PPP and its fluxes due to downregulation of *PGI1* (Qin et al., 2020; Ralser et al., 2007). Indeed,
579   lower glycolysis has been associated with increased oxidative phosphorylation to promote the
580   respiration (Dai et al., 2018) and to improve the stress tolerance (Martínez et al., 2016). This well
581   matches the significant upregulation of the majority of oxidative phosphorylation complexes by

19

582   evolution, as opposed to both evolution and oxidative stress induction, which only slightly

583   upregulated a few corresponding genes including *ATP14*, *COX8* and *VMA6*, while downregulated

584   *PMA1* and *ATP2*, explaining the slightly higher RQ value of E_LRS5. Clearly, upon introducing

585   the exogenous H_2O_2, the correlated flux through glycolysis and the oxidative PPP remained

586   metabolically unchanged, highlighting the robustness of the E_LRS5 upon the oxidative stress re-

587   exposure.

588   Secondly, we noticed the strong upregulation of the nutrient starvation and low-pH induced genes

589   (Zuzuarregui and del Olmo, 2004) *SPI1* and *YGP1* (LFC: 1.44 and 2.06, respectively). SPI1 is a

590   weak acid stress-induced enzyme which through the cell wall remodelling, it improves the cell

591   viability and minimises the plasma membrane damage (Simões et al., 2006) and its

592   overexpression leads to pseudohyphal growth (Cardona et al., 2012). The overexpression of

593   *YGP1* which is also a yeast cell wall glycoprotein has been linked to a fluffy, non-smooth yeast

594   colony morphology that more readily forms filaments (Kuthan et al., 2003).

595   Thirdly, it is also likely that the signalling pathways have also played a part as according to Hong

596   and Nielsen (Hong and Nielsen, 2013), the evolution on galactose caused mutations in RAS-

597   Protein Kinase A (Ras-PKA) signalling pathway, and not in the galactose pathway. Likewise, we

598   observed the strong upregulation of its flocculin-encoding gene *FLO11* by evolution, while several

599   Mitogen activated protein kinase (MAPK) pathway genes like *SLT2*, *SSK1*, *HOG1*, *YPS1*, *SWI6*,

600   *CDC42*, *MID2*, *STE11*, *ATG33*, and *ROM2* were downregulated opposed to the effect of

601   evolution and oxidative stress.

602   Fourthly, the sensing of nutrient limitation has potentially activated the MAPK cascade sub-

603   pathway known as the cell wall integrity (CWI) pathway, which regulates the filamentous growth

604   pathway (Birkaya et al., 2009). In this regard, however, several cell surface sensors (*SLG1*,

605   *WSC3* and *MID2*) were downregulated, and *PTC1*, with a role in the CWI reduction (Bi and Park,

606   2012; Sanz et al., 2022), was upregulated. Similarly, *PRM5*, known as a marker for CWI

607   activation involved in cell wall biogenesis induction, was one of the most strongly downregulated

608   genes due to evolution (LFC= -2.63), decreasing the possibility of CWI being involved in E_LRS5

609   filamentous growth. On the other hand, the secretory pathway stress and damage to ER quality

610   control can also trigger the CWI pathway and activate the unfolded protein response (UPR) to

611   reduce the cell wall damage and increase the secretory pathway folding capacity (Jiménez-

612   Gutiérrez et al., 2020). This potentially explains the moderate upregulation of genes related to

613   protein sorting into endosome and vacuolar, Golgi and exocyst trafficking as well as the

614   misfolded-protein targeting heat shock proteins HSP42 and HSP26 and oxidative-stress defeating

615   HSP70 isoform, *SSA3* (Gupta et al., 2018; Specht et al., 2011). Indeed, the protein folding and

616   secretion are improved by UPR and heat shock response (HSR), whereby the HSR activates the

617   ubiquitin-proteasome and chaperone to relieve the cell stress (Jiménez-Gutiérrez et al., 2020).

618   Opposed to the sole evolution effect, the cumulative effect of both evolution and oxidative stress

619   induction caused the upregulation of the endoplasmic reticulum protein processing pathway,

620   ubiquitin-mediated proteolysis and endocytosis pathway genes. Hence, apparently, the evolved

621   yeast has devised different protection strategies to deal with the misfolded proteins. It would then

622   be intriguing to imagine that the exogenous oxidative stress application resulted in increased

623   protein degradation to compensate for this extra burden on E_LRS5 which could also contribute

624   to more ROS formation. This clearly shows a combination of the cross-protection and anticipation

625   likely occurred to improve the microbial fitness against the stressor, potentially in favour of the

626   diterpenoids formation. In this regard, compared to LRS5, E_LRSII showed a 1.1-fold higher

627   NGAM flux at SSI, showing that this strain spends higher energy producing the correctly folded

628   protein and potentially reducing the misfolded protein fraction. On the other hand, increased

629   respiration brought forward more ATP yield and hence a balance between ATP production and

630   ribosome biosynthesis was needed. In this regard, we noticed that the cytosolic ribosome

631   biogenesis genes were downregulated, while the mitochondrial ribosomal biogenesis genes were

632   upregulated by evolution, the opposite of which was observed by the cumulative effect of both

633   evolution and oxidative stress induction, likely due to the already high availability of them due to

634   evolution. Indeed, respiration is less proteome-efficient than fermentation (Elsemman et al., 2022)

635   and ribosome synthesis can limit the growth (Pfeiffer and Morley, 2014). It is however worth

636   noting that the yeast produces a surplus of ribosomes during stressful conditions to quickly use

637   them for fast growth upon shifting to the normal condition (Metzl-Raz et al., 2017). Despite not

638   having studied the proteomes of the studied conditions, apparently, the ribosome biogenesis

639   likely favoured the respiratory processes rather than the metabolic pathways in E_LRS5, an

640   approach LRS5 strain followed to respond to three different factors of taxadiene, galactose and

641   oxidative stress while minimising its enzymatic costs to further couple its productivity with its

642   growth. We can therefore postulate that the enzymatic contents related to taxadiene synthesis

643   were favoured with sufficient ribosome biosynthesis, lipid and vesicular machinery while reducing

644   the proteome allocation costs for metabolic pathways like glycolysis, resulting in E_LRS5 faster

645   growth rate at our initial experiments (Dai et al., 2018).

646   **3-4. The decreased purine biosynthesis and increased cell cycle arrest and**
647   **hydrophilins expressions likely promoted the antioxidant defence mechanism and**
648   **longevity in H_2O_2 and galactose-adapted yeast**

649   We also noticed the downregulation of gene expression and reaction flux through glycine-
650   cleaving GCVs in the folate cycle, which denote the nitrogen source sufficiency in E_LRS5 SSI,
651   preventing the glycine catabolism (Piper et al., 2002). Likewise, there was a drop in purine
652   biosynthesis, likely to prevent the excess ATP production, and this was particularly more evident
653   for E_LRS5 SSII than that of LRS5. Previous studies have illustrated that purine starvation results
654   in increased oxidative stress tolerance and the cell cycle arrest (Kokina et al., 2019; Ozolina et
655   al., 2017). We can then hypothesise that the downregulated purine biosynthesis together with any
656   nutrient starvation and galactose supplementation, all have contributed to the improved
657   survivability and potential cell cycle arrest to promote yeast longevity and the antioxidant events
658   (Petti et al., 2011), representing an active budding phenotype and causing the activation of the
659   non-respiratory mitochondrial genes (Petti et al., 2011). As a result, mitophagy, a quality control
660   process for the degradation of damaged mitochondria to suppress the mitochondrial ROS
661   accumulation (Kanki et al., 2015), was significantly enriched considering both evolution and
662   oxidative stress effects. Moreover, the evolution upregulated the glutaredoxins and glutathione S-
663   transferases, as the yeast's major antioxidant machinery, together with thioredoxins and
664   glutathione/ glutaredoxins (Grant, 2001). In this regard, the mitochondrial thioredoxin reductase
665   *TRX3*, was significantly upregulated, indicating the long-term adaptation mainly affected the
666   mitochondrial thioredoxin system (Cheng et al., 2019), while both evolution and oxidative stress
667   likely affected the cytosolic thioredoxin system by upregulating *TRX1*. Similarly, the sodium and
668   potassium ATPases, known to protect against the induced cell death (Hoeberichts et al., 2010)
669   were amongst the most highly downregulated genes by the evolution (LFC: -1.67, -1.91, -1.85
670   and -1.12, respectively). Likewise, hydrophilin genes (induced under the dehydration stress)
671   (*SIP18*; LFC: 3.17, *STF2*; LFC: 0.54, *GRE1*; LFC: 1.91) were strongly upregulated by evolution.
672   *SIP18* is known to reduce the H_2O_2-induced yeast apoptosis (Rodríguez-Porrata et al., 2012) and
673   *GRE1* and *STF2* can confer antioxidant capacity as they have been associated with increased
674   cell viability upon restoring the rehydration (López-Martínez et al., 2012).

675   **3-5. Taxadiene has antioxidant properties and the improved TCA cycle activity likely**
676   **provides the required NADPH for diterpenoids production by H_2O_2 and galactose-**
677   **adapted yeast**

678   Overexpressing the phosphoketolase and transaldolase in PPP downstream has been shown to
679   increase the NADPH capability (R. Chen et al., 2022). Also, acute oxidative stress induction was

22

680   shown to inhibit glycolysis, but increasing the PPP metabolism in Hayes et al. study (Hayes et al.,

681   2020). NADPH is also a redox sink, whereby its consumption elevates during oxidative stress as

682   a means of detoxification (Pollak et al., 2007) and the Taxol® cytochrome P450 enzymes like

683   CYP725A4 also rely on its electrons to activate the dioxygen molecule for diterpenoids

684   production. Hence, we could assume that the oxidative stress likely benefits the Taxol® P450s

685   activity in future aside from the other advantages we stated earlier.

686   As illustrated in Figure 4, herein, we noticed the downregulation of NADPH-producing *ZWF1*,

687   *ALD6*, *ALD5*, *GND1*, *TKL1* and *RPE1*, the deletion of the last three been reported to increase the

688   sensitivity to hydrogen peroxide (Thorpe et al., 2004). In contrast, the other NADPH-producing

689   enzymes, cytosolic IDP2 and peroxisomal IDP3 isocitrate dehydrogenases belonging to the TCA

690   cycle were upregulated, denoting that the TCA cycle is responsible for the NADPH generation in

691   the evolved strain, where most TCA cycle genes and reaction fluxes were upregulated. Also, the

692   evolution caused a general downregulation of arginine, alanine, lysine, leucine, and tryptophan

693   biosynthesis genes. It is known that proline, serine and alanine catabolism and decreased

694   arginine biosynthesis can help in ATP regeneration through TCA cycle (Liang et al., 2014) and

695   proline is known to act as the oxidative and osmotic stress protectant (Liang et al., 2014). Also,

696   decreased arginine and sulphur amino acid biosynthesis are known to promote lipid biosynthesis

697   and oxidative stress reduction for recombinant protein production (X. Chen et al., 2022). The

698   polyamines exporter protein-encoding *TPO1* and ornithine decarboxylase *SPE1* were also

699   downregulated, both known to be activated during oxidative stress to increase the lysine uptake

700   from medium to free up NADPH for antioxidant system (Olin-Sandoval et al., 2019). This denotes

701   the sufficiency of NADPH cofactor in E_LRS5 strain as indicated previously. However, we noticed

702   an upregulation of the sulphur assimilation pathway genes acting upstream to the antioxidant

703   enzymes. Therefore, our previous assumption for increasing the oxidative stress as a proxy for

704   higher NADPH availability was partly true, as the upregulation of the NADPH-requiring amino acid

705   biosynthesis and sulphur assimilation pathways both pinpoint to the NADPH inadequacy (Ask et

706   al., 2013).

707   As the expression of their genes remained unchanged due to both evolution and oxidative stress

708   effects, it is therefore likely that the NADPH sources would still be abundant for CYP725A4

709   activity, however, further experiments would still be needed. We, nevertheless, found a significant

710   general downregulation in the early MVA pathway, forming the backbone of the Taxol®

711   precursors, and NADPH-requiring fatty acid biosynthesis genes expression and reaction fluxes,

712   except for *ERG8* and *MVD1*, catalysing the conversion of mevalonate-P mevalonate-PP and to

713   IPP/DMAPP. Nevertheless, both evolution and oxidative stress induction upregulated the

714 expression of *ERG3*, *ERG7* and *ERG27* (Figure 4). Besides giving strength and fluidity to yeast

715 cell membranes, ergosterols have been reported to increase yeast resistance towards different

716 lignocellulosic inhibitors (Endo et al., 2008). The downregulation in this pathway was contrary to

717 our previous strategy of overexpressing its genes for improving the taxadiene titre (Nowrouzi et

718 al., 2020) as well as to Hong et al. study (Hong et al., 2011), where galactose adaptation

719 upregulated the ergosterol pathway. Furthermore, as the excess NADPH is known to be spent in

720 the ergosterol pathway to counteract its harmful effect, there is a possibility that either E_LRS5

721 does not over-accumulate the NADPH, or the evolved cell prioritises its use for other biological

722 processes. In this regard, we however observed that *LPP1* and *DPP1*, catalysing the conversion

723 of GGPP to GGOH (Song et al., 2017), were upregulated by the evolution, possibly indicating the

724 GGPP overaccumulation (Nowrouzi et al., 2020) despite the MVA pathway downregulation. Since

725 we observed higher GGOH and taxadiene titre in E_LRS5, it is plausible that yeast already

726 possessed a more active MVA pathway which necessitated its strong downregulation to reduce

727 the toxicity of its products. A recent study by Jeong et al. (Jeong et al., 2021) also mentioned

728 GGPP toxicity in *E. coli; therefore,* it is likely that the increased GGOH titre was to counteract the
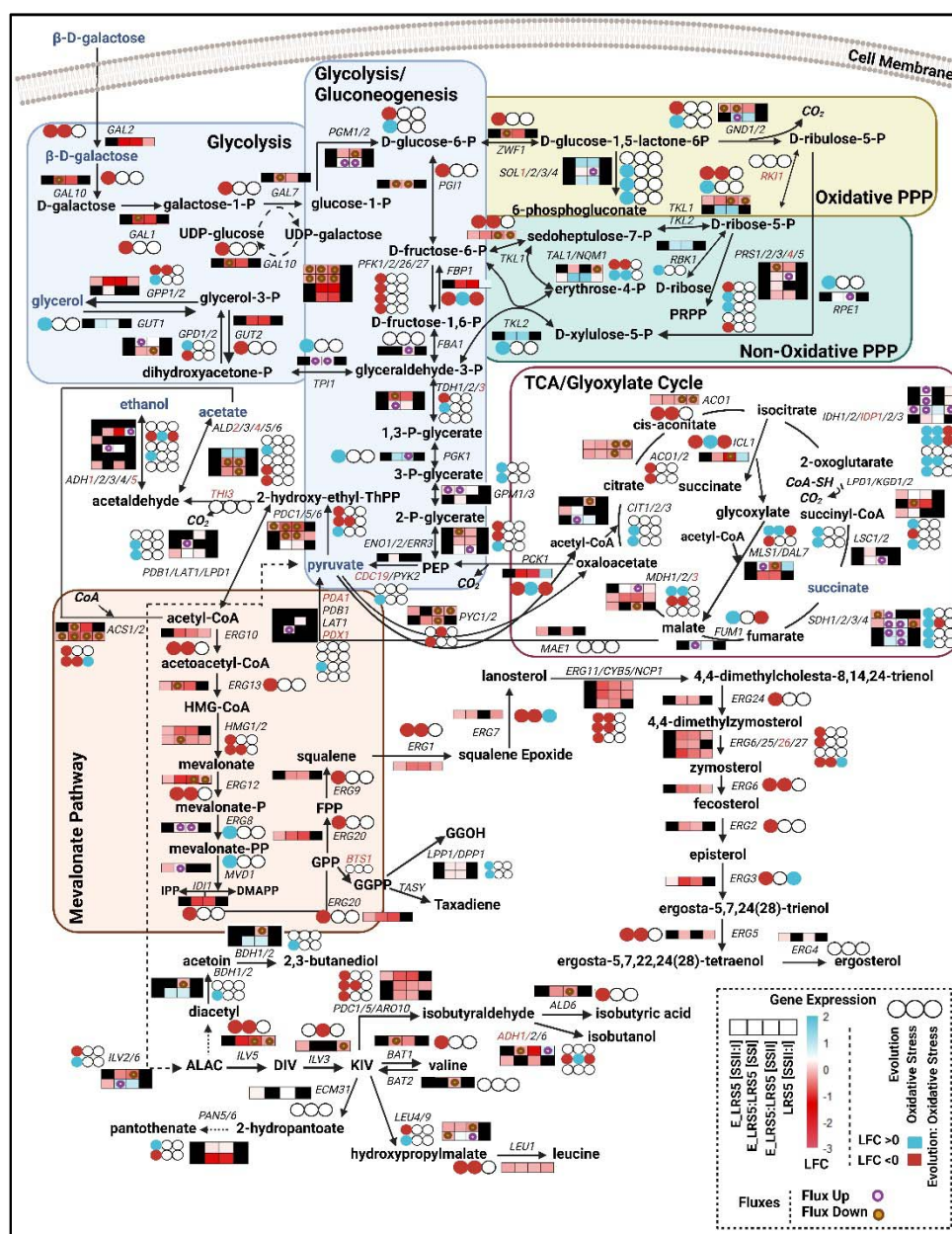
729 excess GGPP toxicity.

730

731 Figure 4. **Effect of the adaptive laboratory evolution and oxidative stress on the central carbon**
732 **metabolism gene expression and flux changes.** The mevalonate pathway produces the precursors to
733 terpene and ergosterol biosynthesis. Significant changes to the gene expression and fluxes (mean of n =
734 10,000 random samples) were selected at log2 fold change = 0 and fold change = 1, respectively, with FDR <
735 0.05. The heatmap boxes show the following pairwise gene expression and flux comparisons from left to right
736 (changes with regards to oxidative stress induction in E_LRS5; changes with regards to evolution only (during
737 steady state I); changes with regards to evolution effect during steady state II; changes with regards to
738 oxidative stress induction in LRS5). The black colour in the heatmaps shows no significant changes to the

25

739   expression of the genes at the specific contrast level. The differential gene expressions were also examined by

740   the effect of evolution, oxidative stress and their interplay and are displayed by triple circles in the order of left

741   to right, where the upregulation and downregulation of the genes are shown with blue and red colours,

742   respectively. Genes without significant expression change at any comparison were highlighted in red. The

743   white colour in the triple circles denotes no significant changes to the expression of the genes with respect to

744   condition variables. Where the flux changes were increased or decreased compared to the control level by their

745   genes, it was shown with purple and yellow circles, respectively. The -P stands for phosphate for all metabolites.

746   Figure was created with BioRender.com.

747

748   **3-6. The oxidative stress re-induction in H_2O_2 and galactose-adapted taxadiene-**

749   **producing yeast likely promotes the flavin formation in favour of CYP725A4**

750   Taxadiene is the substrate to Taxol® CYP725A4 and its interacting reductase POR, each

751   functioning through their prosthetic groups, being heme and flavins, respectively. In addition, the

752   efficient assembly of the cofactor-requiring components of the electron transfer chain (ETC),

753   active in mitochondrial respiration, relies on both mitochondrial flavin adenine dinucleotide (FAD)

754   import, and heme synthesis. We, therefore, studied the changes to biosynthetic pathways of

755   these cofactors to answer if E_LRS5 suited the integration of the later P450 enzyme(s).

756   The flavin-dependent enzymes, mainly located in mitochondria, constitute about 1.1% of the total

757   yeast proteome, with the majority requiring FAD and the rest depending on flavin mononucleotide

758   (FMN), both formed initially from riboflavin (Gudipati et al., 2014). Briefly, the riboflavin

759   biosynthesis forms through the conversion of guanosine triphosphate (GTP) or ribulose 5-

760   phosphate to its intermediate or through direct riboflavin uptake from the medium via plasma

761   membrane flavin transporter MCH5 (Spitzner et al., 2008). This is followed by the enzymatic

762   steps encoded by *RIBs*, and then the activity of the riboflavin kinase (FMN1) to synthesise the

763   FMN and its conversion into FAD in mitochondria by FAD synthase (FAD1) and its export into the

764   extramitochondrial phase via FLX1 FAD transporter enzyme (Bafunno et al., 2004).

765   The Flavin cofactor availability is of extreme importance, where for instance the increased

766   phenolic acids titre was achieved by overexpression of *MCH5*, *RIB1* and *FLX1* (R. Chen et al.,

767   2022). While riboflavin has been reported to increase the resistance against the H_2O_2 (Maslanka

768   and Zadrag-Tecza, 2022), in our study, except *RIB7* and its reaction flux that was upregulated,

769   other RIBs including *RIB1*, *RIB4* and *RIB5* as well as the putative endoplasmic reticulum-

770   associated FAD transporters *FLC1* and *FLC2* and the mitochondrial FAD transporter *FLX1*, were

771   all downregulated by evolution, potentially denoting the lower availability of the mitochondrial FAD

772   in E_LRS5 compared to LRS5. In contrast, the interaction of the evolution and oxidative stress

773   both resulted in increased expression of *RIB4* and *RIB5*, potentially highlighting the
774   overaccumulation of FMN and FAD precursors by the evolution that would suffice at the SSII
775   (Figure 5A). Also, at SSII, only *RIB5* and *FMN1* were upregulated, potentially to counteract the
776   extra stress burden that needed to be compensated with the FMN availability (Chen et al., 2020).
777   While our earlier study did not show any significant effect from FMN on diterpenoid production,
778   others have reported on its remarkable toxicity reduction capability in yeast (Chen et al., 2020; X.
779   Chen et al., 2022). Hence, we can speculate that E_LRS5 likely better serves the expression of
780   Taxol® P450 genes like CYP725A4, despite observing no changes in *FAD1* expression and its
781   promoting effect on increased biomass and diterpenoids production and electron transfer
782   (Gudipati et al., 2014). However, there is also a possibility that the FAD was already highly
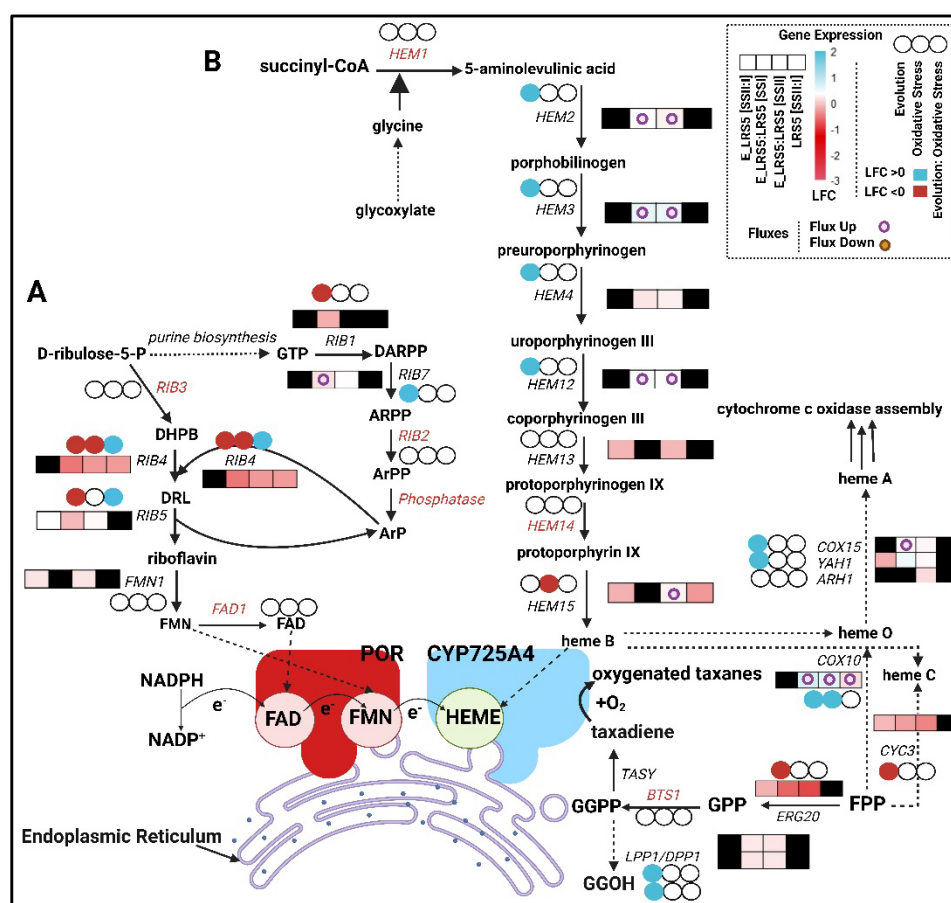783   available, and the earlier steps were rate-limiting for its higher production.

784

785

786   Figure 5. **Riboflavin and heme synthesis flux and expression profile alterations with respect to**
787   **evolution and oxidative stress induction for A) flavin and B) heme biosynthesis.** Significant changes to

788   the gene expression and fluxes (mean of n=10,000 random samples) were selected at log2 fold change = 0

789   and fold change = 1, respectively, with FDR < 0.05. The heatmap boxes show the following pairwise gene

790   expression and flux comparisons from left to right (changes with regards to oxidative stress induction in

791   E_LRS5; changes with regards to evolution only (during steady state I); changes with regards to evolution

792   effect during steady state II; changes with regards to oxidative stress induction in LRS5). The black colour in

793   the heatmaps show no significant changes to the expression of the genes at the specific contrast level. The

794   differential gene expressions were also examined by the effect of evolution, oxidative stress and their interplay

795   and are displayed by triple circles in the order of left to right, where the upregulation and downregulation of the

796   genes are shown with blue and red colours, respectively. Genes without significant expression changes at any

797   comparison were highlighted in red. The white colour in the triple circles denote no significant changes to the

798   expression of the genes with respect to condition variables. Where the flux changes were increased or

799   decreased compared to the control level by their genes, it was shown with purple and yellow circles,

800   respectively. The -P stands for phosphate and e$^-$ stands for electron.

801

802   **3-7. The oxidative stress re-induction in H_2O_2 and galactose-adapted taxadiene-**

803   **producing yeast decreased the iron overaccumulation and heme b degradation**

804   In *S. cerevisiae*, the heme synthesis starts with succinyl-CoA and glycine condensation or

805   through importing iron into mitochondria under the iron deficiency (Li et al., 2020). We already

806   observed an upregulation in the TCA cycle succinyl-CoA-producing *LPD1* and *KGD2*, as well as

807   the AGX1, catalysing the formation of glycine from glyoxylate.

808   We set out to investigate the expression changes of genes directly involved in heme b synthesis

809   for its incorporation into the CYP725A4 enzyme. The heme b synthesis goes through the

810   porphyrin metabolism pathway, which was also found to be significantly enriched by the

811   evolution, where the expression and reaction fluxes of *HEM2*, *HEM3*, *HEM4* and *HEM12*, with

812   enzymes involved in synthesising the intermediates to heme b synthesis were all upregulated

813   (Figure 5B). Similar to the metabolic shift from fermentation to respiration that induces the HAP

814   transcription factor to stimulate the heme-requiring respiratory proteins and ETC (Zhang et al.,

815   2017), *HEM2,3* and *12* genes are known to activate the induction of the TCA cycle and oxidative

816   phosphorylation to source more succinyl-CoA for heme synthesis (Zhang et al., 2017), which

817   aligns well with our previous observation: more active respiration in E_LRS5, compared to LRS5.

818   Similarly, heme b-consuming enzymes encoded by heme A: farnesyltransferase *COX10*, heme a

819   synthase *COX15* and mitochondrial ferredoxin *YAH1* were all upregulated by evolution. However,

820   upon introduction of H_2O_2 in E_LRS5 culture, no expression change was detected, except that

821   the heme b-synthesising *HEM1*, *HEM13*, *HEM15* and heme b-consuming *YAH1* expressions

822 were decreased. Indeed, while heme synthesis can benefit the CYP725A4 expression in the
823 Taxol® pathway, we earlier showed that the heme, be it ready heme or heme precursor like 5-
824 aminolevulinate, can negatively result in decreased biomass and diterpenoid formation (Nowrouzi
825 et al., 2022). This, therefore, justifies the increased reaction flux and expression of *HEM2* to
826 consume these iron sources. Interestingly, comparing the LRS5 and E_LRS5 gene expressions
827 upon oxidative stress induction, no changes to *COX10* expression occurred in E_LRS5 and
828 apparently, minimising the heme b degradation can render E_LRS5 a possibly better cell factory
829 for expressing the Taxol® P450 enzymes. Here, we also observed the upregulation of *HAP2*,
830 *HAP3*, *HAP4* and *HAP5* genes due to evolution. *HAP1*, known to induce the expression of the
831 ergosterol biosynthesis and superoxide dismutase genes, was however downregulated,
832 potentially explaining the downregulation of the ergosterol pathway. We, however, can speculate
833 that despite the downregulation of *HAP1*, the upregulation of *HAP2-5* regulated the flux TCA
834 cycle and ETC enzymes (Zhang et al., 2017), while being in accordance with more respiratory
835 status at E_LRS5 during steady state I (SSI). From the other perspective, we can argue that the
836 iron economisation was towards prioritising the expression of H_2O_2-degrading iron-containing
837 catalases like heme b-containing *CTT1* (Cassanova et al., 2005). Similarly, *CCC1*, known to be
838 activated to store the excess iron and defeat the iron toxicity (Li et al., 2017, 2001; Li and Ward,
839 2018) under the excess cytosolic iron availability, was downregulated by evolution, pinpointing to
840 potential iron limitation in the cytosol. Despite this, considering the effect of both evolution and
841 oxidative agent, we observed its upregulation, likely to minimise the ROS generation by excess
842 iron.

4. Conclusions

844 Earlier studies revealed the presence of oxidative stress in *S. cerevisiae* cell factories expressing
845 *Taxus* sp. *CYP725A4* and its cognate reductase gene *POR*, hampering the production of the
846 highly oxygenated anticancer drug, Taxol® precursors in yeast. Using adaptive laboratory
847 evolution, we evolved a taxadiene-producing yeast strain with increased tolerance against
848 hydrogen peroxide (H_2O_2) while growing on a galactose-containing medium. The best-performing
849 evolved strain showed three-fold higher taxadiene titre, and later, decreased overflow metabolites
850 production in galactose-limited chemostat cultures. To mimic the oxidative stress induction, the
851 exometabolic and expression profiles of the best-performing evolved strain and the parent strain
852 before and during the H_2O_2 induction were studied. Integrating these data with an enzyme-
853 constrained metabolic model showed that the evolution caused the strong upregulation of the
854 mitochondrial respiration as well as the downregulation of the glycolysis and mevalonate
855 pathway, the latter forming the geranylgeranyl diphosphate (GGPP) as the taxadiene synthase

856   substrate. This likely indicated that the antioxidant properties of taxadiene caused its higher
857   production or this was to defeat the GGPP toxicity as reported earlier, all of which potentially
858   resulted in high yeast budding and cell cycle arrest as a defence mechanism. The higher
859   respiration was associated with the elevated upregulation of mitochondrial ribosomal and
860   downregulation of the cytosolic ribosomal genes. The upregulation of the TCA cycle and
861   antioxidant machinery and the downregulation of amino acid production, likely pinpoint to the
862   higher NADPH in the evolved strain, which also acts as the cofactor to cytochrome P450
863   enzymes of the Taxol® pathway. The oxidative stress induction also downregulated the heme b
864   biosynthesis and upregulated the flavin biosynthesis, which were earlier reported to improve
865   Taxol® early diterpenoids production. On the other hand, the oxidative stress likely caused higher
866   protein misfolding in the evolved strain, while the re-introduction of the oxidative stress induced
867   the proteasomal degradation, as was with storing the branched oxidant-protecting molecules like
868   trehalose and glycogen and hydrolysing them upon H_2O_2 re-induction. This points to the
869   existence of both cross-protection and anticipation mechanisms that contributed to greater
870   microbial fitness, being beneficial to Taxol® cytochrome P450 enzymes in the long term. Clearly,
871   the presence of mutation(s) have contributed to the better fitness of the evolved strain, which can
872   be further investigated with genome sequencing and reverse engineering in future studies
873   following systematic approaches (Malci et al. 2022b), nevertheless, these were out of the scope
874   of this study. As of now, the expression of Taxol® pathway genes are conveniently controlled by
875   galactose induction in yeast. Hence, changes to cell factory design are suggested to only activate
876   the *CYP725A4-POR* expression upon achieving sufficient intracellular taxadiene level and to
877   allow for yeast to optimise its resources timely and stepwise. On this matter, there is still a need
878   to obtain purified taxadiene to first enable the faster development of specific taxadiene-
879   responsive promoter-based biosensors.

880   **5. Data, Materials, and Software Availability**
881   Upon obtaining formal written consent from the first author, all evolved strains generated in this
882   study can only be made available for non-commercial purposes (Nowrouzi, 2022). The log2 fold
883   changes and adjusted p values for the genes discussed/illustrated in this manuscript are available at
884   https://figshare.com/s/3717f4b900bc19124ea7   (RNA-seq)   and
885   https://figshare.com/s/7bd488ddf6b4516876d8 (flux enrichment analysis). The gene expression datasets
886   are available at Gene Expression Omnibus. All other generated datasets will be made available on
887   the supplementary information or upon request from the corresponding author.

6. References

Agren, R., Liu, L., Shoaie, S., Vongsangnak, W., Nookaew, I., Nielsen, J., 2013. The RAVEN Toolbox and its use for generating a genome-scale metabolic model for Penicillium chrysogenum. PLOS Comput. Biol. 9, e1002980.

Ajikumar, P.K., Xiao, W.-H., Tyo, K.E.J., Wang, Y., Simeon, F., Leonard, E., Mucha, O., Phon, T.H., Pfeifer, B., Stephanopoulos, G., 2010. Isoprenoid pathway optimization for Taxol precursor overproduction in Escherichia coli. Science 330, 70–74. https://doi.org/10.1126/science.1191652

Ask, M., Bettiga, M., Duraiswamy, V.R., Olsson, L., 2013. Pulsed addition of HMF and furfural to batch-grown xylose-utilizing Saccharomyces cerevisiae results in different physiological responses in glucose and xylose consumption phase. Biotechnol. Biofuels 6, 181. https://doi.org/10.1186/1754-6834-6-181

Bafunno, V., Giancaspero, T.A., Brizio, C., Bufano, D., Passarella, S., Boles, E., Barile, M., 2004. Riboflavin uptake and FAD synthesis in Saccharomyces cerevisiae mitochondria: involvement of the Flx1p carrier in FAD export. J. Biol. Chem. 279, 95–102. https://doi.org/10.1074/jbc.M308230200

Barrales-Cureño, H.J., Ramos Valdivia, A.C., Soto Hernández, M., 2022. Increased production of taxoids in suspension cultures of Taxus globosa after elicitation. Futur. Pharmacol. https://doi.org/10.3390/futurepharmacol2010004

Barton, N.A., Marsh, B.J., Lewis, W., Narraidoo, N., Seymour, G.B., Fray, R., Hayes, C.J., 2016. Accessing low-oxidation state taxanes: is taxadiene-4(5)-epoxide on the taxol biosynthetic pathway? Chem. Sci. 7, 3102–3107. https://doi.org/10.1039/C5SC03463A

Benjamini, Y., Hochberg, Y., 1995. Controlling the false discovery rate: A practical and powerful approach to multiple testing. J. R. Stat. Soc. Ser. B 57, 289–300. https://doi.org/https://doi.org/10.1111/j.2517-6161.1995.tb02031.x

Bi, E., Park, H.-O., 2012. Cell polarization and cytokinesis in budding yeast. Genetics 191, 347–387. https://doi.org/10.1534/genetics.111.132886

Birkaya, B., Maddi, A., Joshi, J., Free, S.J., Cullen, P.J., 2009. Role of the cell wall integrity and filamentous growth mitogen-activated protein kinase pathways in cell wall remodeling during

918 filamentous growth. Eukaryot. Cell 8, 1118–1133. https://doi.org/10.1128/EC.00006-09

919 Blaga, A.C., Ciobanu, C., Cașcaval, D., Galaction, A.-I., 2018. Enhancement of ergosterol
920 production by Saccharomyces cerevisiae in batch and fed-batch fermentation processes
921 using n-dodecane as oxygen-vector. Biochem. Eng. J. 131, 70–76.
922 https://doi.org/https://doi.org/10.1016/j.bej.2017.12.010

923 Cardona, F., Del Olmo, M.L., Aranda, A., 2012. Phylogenetic origin and transcriptional regulation
924 at the post-diauxic phase of SPI1, in Saccharomyces cerevisiae. Cell. Mol. Biol. Lett. 17,
925 393–407. https://doi.org/10.2478/s11658-012-0017-4

926 Carlson, M., 2019. org.Sc.sgd.db: Genome wide annotation for yeast.
927 https://doi.org/10.18129/B9.bioc.org.Sc.sgd.db

928 Cassanova, N., O'Brien, K.M., Stahl, B.T., McClure, T., Poyton, R.O., 2005. Yeast
929 flavohemoglobin, a nitric oxide oxidoreductase, is located in both the cytosol and the
930 mitochondrial matrix: effects of respiration, anoxia, and the mitochondrial genome on its
931 intracellular level and distribution. J. Biol. Chem. 280, 7645–7653.
932 https://doi.org/10.1074/jbc.M411478200

933 Chang, A., Jeske, L., Ulbrich, S., Hofmann, J., Koblitz, J., Schomburg, I., Neumann-Schaal, M.,
934 Jahn, D., Schomburg, D., 2021. BRENDA, the ELIXIR core data resource in 2021: new
935 developments and updates. Nucleic Acids Res. 49, D498–D508.
936 https://doi.org/10.1093/nar/gkaa1025

937 Chen, R., Gao, J., Yu, W., Chen, X., Zhai, X., Chen, Y., Zhang, L., Zhou, Y.J., 2022. Engineering
938 cofactor supply and recycling to drive phenolic acid biosynthesis in yeast. Nat. Chem. Biol.
939 18, 520–529. https://doi.org/10.1038/s41589-022-01014-6

940 Chen, X., Ji, B., Hao, X., Li, X., Eisele, F., Nyström, T., Petranovic, D., 2020. FMN reduces
941 Amyloid-β toxicity in yeast by regulating redox status and cellular metabolism. Nat.
942 Commun. 11, 867. https://doi.org/10.1038/s41467-020-14525-4

943 Chen, X., Li, X., Ji, B., Wang, Y., Ishchuk, O.P., Vorontsov, E., Petranovic, D., Siewers, V.,
944 Engqvist, M.K.M., 2022. Suppressors of amyloid-β toxicity improve recombinant protein
945 production in yeast by reducing oxidative stress and tuning cellular metabolism. Metab. Eng.
946 72, 311–324. https://doi.org/https://doi.org/10.1016/j.ymben.2022.04.005

947 Cheng, L., Zhang, X., Zheng, X., Wu, Z., Weng, P., 2019. RNA-seq transcriptomic analysis of
948   green tea polyphenols regulation of differently expressed genes in Saccharomyces
949   cerevisiae under ethanol stress. World J. Microbiol. Biotechnol. 35, 59.
950   https://doi.org/10.1007/s11274-019-2639-4

951 Dai, Z., Huang, M., Chen, Y., Siewers, V., Nielsen, J., 2018. Global rewiring of cellular
952   metabolism renders Saccharomyces cerevisiae Crabtree negative. Nat. Commun. 9, 3059.
953   https://doi.org/10.1038/s41467-018-05409-9

954 de Jongh, W.A., Bro, C., Ostergaard, S., Regenberg, B., Olsson, L., Nielsen, J., 2008. The roles
955   of galactitol, galactose-1-phosphate, and phosphoglucomutase in galactose-induced toxicity
956   in Saccharomyces cerevisiae. Biotechnol. Bioeng. 101, 317–326.
957   https://doi.org/https://doi.org/10.1002/bit.21890

958 Di Tommaso, P., Chatzou, M., Floden, E.W., Barja, P.P., Palumbo, E., Notredame, C., 2017.
959   Nextflow enables reproducible computational workflows. Nat. Biotechnol. 35, 316–319.
960   https://doi.org/10.1038/nbt.3820

961 Domenzain, I., Sánchez, B., Anton, M., Kerkhoven, E.J., Millán-Oropeza, A., Henry, C., Siewers,
962   V., Morrissey, J.P., Sonnenschein, N., Nielsen, J., 2022. Reconstruction of a catalogue of
963   genome-scale metabolic models with enzymatic constraints using GECKO 2.0. Nat.
964   Commun. 13, 3766. https://doi.org/10.1038/s41467-022-31421-1

965 Edgar, S., Zhou, K., Qiao, K., King, J.R., Simpson, J.H., Stephanopoulos, G., 2016. Mechanistic
966   insights into taxadiene epoxidation by taxadiene-5α-hydroxylase. ACS Chem. Biol. 11, 460–
967   469. https://doi.org/10.1021/acschembio.5b00767

968 Elsemman, I.E., Rodriguez Prado, A., Grigaitis, P., Garcia Albornoz, M., Harman, V., Holman,
969   S.W., van Heerden, J., Bruggeman, F.J., Bisschops, M.M.M., Sonnenschein, N., Hubbard,
970   S., Beynon, R., Daran-Lapujade, P., Nielsen, J., Teusink, B., 2022. Whole-cell modeling in
971   yeast predicts compartment-specific proteome constraints that drive metabolic strategies.
972   Nat. Commun. 13, 801. https://doi.org/10.1038/s41467-022-28467-6

973 Endo, A., Nakamura, T., Ando, A., Tokuyasu, K., Shima, J., 2008. Genome-wide screening of the
974   genes required for tolerance to vanillin, which is a potential inhibitor of bioethanol
975   fermentation, in Saccharomyces cerevisiae. Biotechnol. Biofuels 1, 3.
976   https://doi.org/10.1186/1754-6834-1-3

977   Entian, K.-D., Kötter, P., 2007. 25 yeast genetic strain and plasmid Collections, in: Stansfield, I.,
978   Stark, M.J.R.B.T.-M. in M. (Eds.), Yeast Gene Analysis. Academic Press, pp. 629–666.
979   https://doi.org/https://doi.org/10.1016/S0580-9517(06)36025-4

980   Escrich, A., Almagro, L., Moyano, E., Cusido, R.M., Bonfill, M., Hosseini, B., Palazon, J., 2021.
981   Improved biotechnological production of paclitaxel in Taxus media cell cultures by the
982   combined action of coronatine and calix[8]arenes. Plant Physiol. Biochem. 163, 68–75.
983   https://doi.org/https://doi.org/10.1016/j.plaphy.2021.03.047

984   Ewels, P., Magnusson, M., Lundin, S., Käller, M., 2016. MultiQC: summarize analysis results for
985   multiple tools and samples in a single report. Bioinformatics 32, 3047–3048.
986   https://doi.org/10.1093/bioinformatics/btw354

987   Ewels, P.A., Peltzer, A., Fillinger, S., Patel, H., Alneberg, J., Wilm, A., Garcia, M.U., Di Tommaso,
988   P., Nahnsen, S., 2020. The nf-core framework for community-curated bioinformatics
989   pipelines. Nat. Biotechnol. 38, 276–278. https://doi.org/10.1038/s41587-020-0439-x

990   Galindo-Rodriguez, G. R., Santoyo-Garcia, J.H., Rios-Solis, L., Dimartino, S. 2023. *In*
991   *situ recovery of taxadiene using solid adsorption in cultivations with Saccharomyces*
992   *cerevisiae. Prep. Biochem. Biotechnol. 1-9.*
993   https://doi.org/10.1080/10826068.2023.2207204

994   Garrido, E.O., Grant, C.M., 2002. Role of thioredoxins in the response of Saccharomyces
995   cerevisiae to oxidative stress induced by hydroperoxides. Mol. Microbiol. 43, 993–1003.
996   https://doi.org/10.1046/j.1365-2958.2002.02795.x

997   Grant, C.M., 2001. Role of the glutathione/glutaredoxin and thioredoxin systems in yeast growth
998   and response to stress conditions. Mol. Microbiol. 39, 533–541.
999   https://doi.org/https://doi.org/10.1046/j.1365-2958.2001.02283.x

1000   Gudipati, V., Koch, K., Lienhart, W.-D., Macheroux, P., 2014. The flavoproteome of the yeast
1001   Saccharomyces cerevisiae. Biochim. Biophys. Acta 1844, 535–544.
1002   https://doi.org/10.1016/j.bbapap.2013.12.015

1003   Gupta, A., Puri, A., Singh, P., Sonam, S., Pandey, R., Sharma, D., 2018. The yeast stress
1004   inducible Ssa Hsp70 reduces α-synuclein toxicity by promoting its degradation through
1005   autophagy. PLOS Genet. 14, e1007751.

1006 Hayes, J.D., Dinkova-Kostova, A.T., Tew, K.D., 2020. Oxidative stress in cancer. Cancer Cell 38,
1007   167–197. https://doi.org/https://doi.org/10.1016/j.ccell.2020.06.001

1008 Heirendt, L., Arreckx, S., Pfau, T., Mendoza, S.N., Richelle, A., Heinken, A., Haraldsdóttir, H.S.,
1009   Wachowiak, J., Keating, S.M., Vlasov, V., Magnusdóttir, S., Ng, C.Y., Preciat, G., Žagare,
1010   A., Chan, S.H.J., Aurich, M.K., Clancy, C.M., Modamio, J., Sauls, J.T., Noronha, A.,
1011   Bordbar, A., Cousins, B., El Assal, D.C., Valcarcel, L. V, Apaolaza, I., Ghaderi, S.,
1012   Ahookhosh, M., Ben Guebila, M., Kostromins, A., Sompairac, N., Le, H.M., Ma, D., Sun, Y.,
1013   Wang, L., Yurkovich, J.T., Oliveira, M.A.P., Vuong, P.T., El Assal, L.P., Kuperstein, I.,
1014   Zinovyev, A., Hinton, H.S., Bryant, W.A., Aragón Artacho, F.J., Planes, F.J., Stalidzans, E.,
1015   Maass, A., Vempala, S., Hucka, M., Saunders, M.A., Maranas, C.D., Lewis, N.E., Sauter, T.,
1016   Palsson, B.Ø., Thiele, I., Fleming, R.M.T., 2019. Creation and analysis of biochemical
1017   constraint-based models using the COBRA Toolbox v.3.0. Nat. Protoc. 14, 639–702.
1018   https://doi.org/10.1038/s41596-018-0098-2

1019 Hoeberichts, F.A., Perez-Valle, J., Montesinos, C., Mulet, J.M., Planes, M.D., Hueso, G., Yenush,
1020   L., Sharma, S.C., Serrano, R., 2010. The role of K+ and H+ transport systems during
1021   glucose- and H2O2-induced cell death in Saccharomyces cerevisiae. Yeast 27, 713–725.
1022   https://doi.org/https://doi.org/10.1002/yea.1767

1023 Hong, K.-K., Nielsen, J., 2013. Adaptively evolved yeast mutants on galactose show trade-offs in
1024   carbon utilization on glucose. Metab. Eng. 16, 78–86.
1025   https://doi.org/https://doi.org/10.1016/j.ymben.2013.01.007

1026 Hong, K.-K., Vongsangnak, W., Vemuri, G.N., Nielsen, J., 2011. Unravelling evolutionary
1027   strategies of yeast for improving galactose utilization through integrated systems level
1028   analysis. Proc. Natl. Acad. Sci. U. S. A. 108, 12179–12184.
1029   https://doi.org/10.1073/pnas.1103219108

1030 Jeong, S.-H., Park, J.-B., Wang, Y., Kim, G.-H., Zhang, G., Wei, G., Wang, C., Kim, S.-W., 2021.
1031   Regulatory molecule cAMP changes cell fitness of the engineered Escherichia coli for
1032   terpenoids production. Metab. Eng. 65, 178–184.

1033 Jiménez-Gutiérrez, E., Alegría-Carrasco, E., Sellers-Moya, Á., Molina, M., Martín, H., 2020. Not
1034   just the wall: the other ways to turn the yeast CWI pathway on. Int. Microbiol. Off. J.
1035   Spanish Soc. Microbiol. 23, 107–119. https://doi.org/10.1007/s10123-019-00092-2

1036 Jongedijk, E., Cankar, K., Ranzijn, J., van der Krol, S., Bouwmeester, H., Beekwilder, J., 2015.

1037   Capturing of the monoterpene olefin limonene produced in Saccharomyces cerevisiae.
1038   Yeast 32, 159–171. https://doi.org/10.1002/yea.3038

1039 Kanehisa, M., Goto, S., 2000. KEGG: kyoto encyclopedia of genes and genomes. Nucleic Acids
1040   Res. 28, 27–30. https://doi.org/10.1093/nar/28.1.27

1041 Kanki, T., Furukawa, K., Yamashita, S., 2015. Mitophagy in yeast: Molecular mechanisms and
1042   physiological role. Biochim. Biophys. Acta - Mol. Cell Res. 1853, 2756–2765.
1043   https://doi.org/https://doi.org/10.1016/j.bbamcr.2015.01.005

1044 Ketchum, R.E., Gibson, D.M., Croteau, R.B., Shuler, M.L., 1999. The kinetics of taxoid
1045   accumulation in cell suspension cultures of Taxus following elicitation with methyl
1046   jasmonate. Biotechnol. Bioeng. 62, 97–105. https://doi.org/10.1002/(sici)1097-
1047   0290(19990105)62:1<97::aid-bit11>3.0.co;2-c

1048 Kim, J., Darlington, A., Salvador, M., Utrilla, J., Jiménez, J.I., 2020. Trade-offs between gene
1049   expression, growth and phenotypic diversity in microbial populations. Curr. Opin. Biotechnol.
1050   62, 29–37. https://doi.org/https://doi.org/10.1016/j.copbio.2019.08.004

1051 Kocaefe-Özşen, N., Yilmaz, B., Alkım, C., Arslan, M., Topaloğlu, A., Kısakesen, H. I□brahim,
1052   Gülsev, E., Çakar, Z.P., 2022. Physiological and molecular characterization of an oxidative
1053   stress-resistant Saccharomyces cerevisiae strain obtained by evolutionary engineering.
1054   Front. Microbiol.

1055 Kokina, A., Ozolina, Z., Liepins, J., 2019. Purine auxotrophy: Possible applications beyond
1056   genetic marker. Yeast 36, 649–656. https://doi.org/https://doi.org/10.1002/yea.3434

1057 Kussell, E., 2013. Evolution in Microbes. Annu. Rev. Biophys. 42, 493–514.
1058   https://doi.org/10.1146/annurev-biophys-083012-130320

1059 Kuthan, M., Devaux, F., Janderová, B., Slaninová, I., Jacq, C., Palková, Z., 2003. Domestication
1060   of wild Saccharomyces cerevisiae is accompanied by changes in gene expression and
1061   colony morphology. Mol. Microbiol. 47, 745–754.
1062   https://doi.org/https://doi.org/10.1046/j.1365-2958.2003.03332.x

1063 Lange, B.M., Conner, C.F., 2021. Taxanes and taxoids of the genus Taxus – A comprehensive
1064   inventory of chemical diversity. Phytochemistry 190, 112829.
1065   https://doi.org/https://doi.org/10.1016/j.phytochem.2021.112829

1066   Li, L., Bertram, S., Kaplan, J., Jia, X., Ward, D.M., 2020. The mitochondrial iron exporter genes
1067   MMT1 and MMT2 in yeast are transcriptionally regulated by Aft1 and Yap1. J. Biol. Chem.
1068   295, 1716–1726. https://doi.org/10.1074/jbc.RA119.011154

1069   Li, L., Chen, O.S., McVey Ward, D., Kaplan, J., 2001. CCC1 is a transporter that mediates
1070   vacuolar iron storage in yeast. J. Biol. Chem. 276, 29515–29519.
1071   https://doi.org/10.1074/jbc.M103944200

1072   Li, L., Kaplan, J., Ward, D.M., 2017. The glucose sensor Snf1 and the transcription factors Msn2
1073   and Msn4 regulate transcription of the vacuolar iron importer gene CCC1 and iron
1074   resistance in yeast. J. Biol. Chem. 292, 15577–15586.
1075   https://doi.org/10.1074/jbc.M117.802504

1076   Li, L., Ward, D.M., 2018. Iron toxicity in yeast: transcriptional regulation of the vacuolar iron
1077   importer Ccc1. Curr. Genet. 64, 413–416. https://doi.org/10.1007/s00294-017-0767-7

1078   Liang, X., Dickman, M.B., Becker, D.F., 2014. Proline biosynthesis is required for endoplasmic
1079   reticulum stress tolerance in Saccharomyces cerevisiae. J. Biol. Chem. 289, 27794–27806.
1080   https://doi.org/10.1074/jbc.M114.562827

1081   López-Martínez, G., Rodríguez-Porrata, B., Margalef-Català, M., Cordero-Otero, R., 2012. The
1082   STF2p Hydrophilin from Saccharomyces cerevisiae Is Required for Dehydration Stress
1083   Tolerance. PLoS One 7, e33324.

1084   Love, M.I., Huber, W., Anders, S., 2014. Moderated estimation of fold change and dispersion for
1085   RNA-seq data with DESeq2. Genome Biol. 15, 550. https://doi.org/10.1186/s13059-014-
1086   0550-8

1087   Malcı, K., Jonguitud-Borrego, N., Van der Straten Waillet, U., Puodziunaite, U., Johnston, E.J.,
1088   Rosser, S.J., Rios-Solis, L. 2022. ACtivE: Assembly and CRISPR-Targeted in Vivo Editing
1089   for Yeast Genome Engineering Using Minimum Reagents and Time. ACS Synth. Biol.11.
1090   3629-3643. https://doi.org/10.1021/acssynbio.2c00175

1091   Malcı, K., Watts, E., Michelle Roberts, T.,Yam Auxillos, J., Nowrouzi, B., Oss Boll, H., Zolnier
1092   Sousa do Nascimento, C., Andreou, A., Vegh, P., Donovan, S., Fragkoudis, R., Panke, S.,
1093   Wallace, E., Elfick, A., Rios-Solis, L. 2022b. Standardization of Synthetic Biology Tools
1094   and Assembly Methods for Saccharomyces cerevisiae and Emerging Yeast Species. ACS
1095   Synth. Biol. 11, 2527–2547. https://doi.org/10.1021/acssynbio.1c00442

1096   Martin, V.J.J., Pitera, D.J., Withers, S.T., Newman, J.D., Keasling, J.D., 2003. Engineering a
1097   mevalonate pathway in Escherichia coli for production of terpenoids. Nat. Biotechnol. 21,
1098   796–802. https://doi.org/10.1038/nbt833

1099   Martínez, J.L., Meza, E., Petranovic, D., Nielsen, J., 2016. The impact of respiration and oxidative
1100   stress response on recombinant α-amylase production by Saccharomyces cerevisiae.
1101   Metab. Eng. Commun. 3, 205–210.
1102   https://doi.org/https://doi.org/10.1016/j.meteno.2016.06.003

1103   Maslanka, R., Zadrag-Tecza, R., 2022. Different life strategies in genetic backgrounds of the
1104   Saccharomyces cerevisiae yeast cells. Fungal Biol. 126, 498–510.
1105   https://doi.org/https://doi.org/10.1016/j.funbio.2022.04.004

1106   McGarrity, S., Karvelsson, S.T., Sigurjónsson, Ó.E., Rolfsson, Ó., 2020. Comparative Metabolic
1107   Network Flux Analysis to Identify Differences in Cellular Metabolism. Methods Mol. Biol.
1108   2088, 223–269. https://doi.org/10.1007/978-1-0716-0159-4_11

1109   McNeil, J.B., McIntosh, E.M., Taylor, B. V, Zhang, F.R., Tang, S., Bognar, A.L., 1994. Cloning
1110   and molecular characterization of three genes, including two genes encoding serine
1111   hydroxymethyltransferases, whose inactivation is required to render yeast auxotrophic for
1112   glycine. J. Biol. Chem. 269, 9155–9165.

1113   Metzl-Raz, E., Kafri, M., Yaakov, G., Soifer, I., Gurvich, Y., Barkai, N., 2017. Principles of cellular
1114   resource allocation revealed by condition-dependent proteome profiling. Elife 6.
1115   https://doi.org/10.7554/eLife.28034

1116   Mirjalili, N., Linden, J.C., 1996. Methyl jasmonate induced production of taxol in suspension
1117   cultures of Taxus cuspidata: ethylene interaction and induction models. Biotechnol. Prog.
1118   12, 110–118. https://doi.org/10.1021/bp9500831

1119   Mohammad, K., Baratang Junio, J.A., Tafakori, T., Orfanos, E., Titorenko, V.I., 2020.
1120   Mechanisms that link chronological aging to cellular quiescence in budding yeast. Int. J.
1121   Mol. Sci. https://doi.org/10.3390/ijms21134717

1122   Nowrouzi, B., 2022. Design of microbial cell factories using integrated synthetic biology and
1123   systems biology for the production of Taxol®, an anticancer drug. The University of
1124   Edinburgh.

1125   Nowrouzi, B., Li, R.A., Walls, L.E., d'Espaux, L., Malcı, K., Liang, L., Jonguitud-Borrego, N.,
1126   Lerma-Escalera, A.I., Morones-Ramirez, J.R., Keasling, J.D., Rios-Solis, L., 2020.
1127   Enhanced production of taxadiene in Saccharomyces cerevisiae. Microb. Cell Fact. 19, 200.
1128   https://doi.org/10.1186/s12934-020-01458-2

1129   Nowrouzi, B., Lungang, L., Rios-Solis, L., 2022. Exploring optimal Taxol® CYP725A4 activity in
1130   Saccharomyces cerevisiae. Microb. Cell Fact. 21, 197. https://doi.org/10.1186/s12934-022-
1131   01922-1

1132   Nowrouzi, B., Rios-Solis, L., 2021. Redox metabolism for improving whole-cell P450-catalysed
1133   terpenoid biosynthesis. Crit. Rev. Biotechnol. 1–25.
1134   https://doi.org/10.1080/07388551.2021.1990210

1135   Olin-Sandoval, V., Yu, J.S.L., Miller-Fleming, L., Alam, M.T., Kamrad, S., Correia-Melo, C., Haas,
1136   R., Segal, J., Peña Navarro, D.A., Herrera-Dominguez, L., Méndez-Lucio, O., Vowinckel, J.,
1137   Mülleder, M., Ralser, M., 2019. Lysine harvesting is an antioxidant strategy and triggers
1138   underground polyamine metabolism. Nature 572, 249–253. https://doi.org/10.1038/s41586-
1139   019-1442-6

1140   Ostergaard, S., Olsson, L., Johnston, M., Nielsen, J., 2000. Increasing galactose consumption by
1141   Saccharomyces cerevisiae through metabolic engineering of the GAL gene regulatory
1142   network. Nat. Biotechnol. 18, 1283–1286. https://doi.org/10.1038/82400

1143   Ozolina, Z., Kokina, A., Liepins, J., 2017. Adenine starvation is signalled through environmental
1144   stress response system in budding yeast Saccharomyces cerevisiae. Environ. Exp. Biol.
1145   283–288.

1146   Patro, R., Duggal, G., Love, M.I., Irizarry, R.A., Kingsford, C., 2017. Salmon provides fast and
1147   bias-aware quantification of transcript expression. Nat. Methods 14, 417–419.
1148   https://doi.org/10.1038/nmeth.4197

1149   Paulo, J.A., O'Connell, J.D., Gaun, A., Gygi, S.P., 2015. Proteome-wide quantitative multiplexed
1150   profiling of protein expression: carbon-source dependency in Saccharomyces cerevisiae.
1151   Mol. Biol. Cell 26, 4063–4074. https://doi.org/10.1091/mbc.E15-07-0499

1152   Petti, A.A., Crutchfield, C.A., Rabinowitz, J.D., Botstein, D., 2011. Survival of starving yeast is
1153   correlated with oxidative stress response and nonrespiratory mitochondrial function. Proc.
1154   Natl. Acad. Sci. U. S. A. 108, E1089-98. https://doi.org/10.1073/pnas.1101494108

1155   Petzoldt, T., 2020. growthrates: Estimate growth rates from experimental Data.

1156   Pfeiffer, T., Morley, A., 2014. An evolutionary perspective on the Crabtree effect. Front. Mol.
1157   Biosci. 1, 17. https://doi.org/10.3389/fmolb.2014.00017

1158   Piper, M.D.W., Hong, S.P., Eissing, T., Sealey, P., Dawes, I.W., 2002. Regulation of the yeast
1159   glycine cleavage genes is responsive to the availability of multiple nutrients. FEMS Yeast
1160   Res. 2, 59–71. https://doi.org/10.1111/j.1567-1364.2002.tb00069.x

1161   Pollak, N., Dölle, C., Ziegler, M., 2007. The power to reduce: pyridine nucleotides – small
1162   molecules with a multitude of functions. Biochem. J. 402, 205–218.
1163   https://doi.org/10.1042/BJ20061638

1164   Qin, N., Li, L., Ji, X., Li, X., Zhang, Y., Larsson, C., Chen, Y., Nielsen, J., Liu, Z., 2020. Rewiring
1165   central carbon metabolism ensures increased provision of acetyl-CoA and NADPH required
1166   for 3-oh-propionic acid production. ACS Synth. Biol. 9, 3236–3244.
1167   https://doi.org/10.1021/acssynbio.0c00264

1168   Queiroz, M.G., Elsztein, C., de Morais, M.A.J., 2020. The effects of the Ncw2 protein of
1169   Saccharomyces cerevisiae on the positioning of chitin in response to cell wall damage.
1170   Antonie Van Leeuwenhoek 113, 265–277. https://doi.org/10.1007/s10482-019-01335-y

1171   Ralser, M., Wamelink, M.M., Kowald, A., Gerisch, B., Heeren, G., Struys, E.A., Klipp, E., Jakobs,
1172   C., Breitenbach, M., Lehrach, H., Krobitsch, S., 2007. Dynamic rerouting of the
1173   carbohydrate flux is key to counteracting oxidative stress. J. Biol. 6, 10.
1174   https://doi.org/10.1186/jbiol61

1175   Reider Apel, A., d'Espaux, L., Wehrs, M., Sachs, D., Li, R.A., Tong, G.J., Garber, M., Nnadi, O.,
1176   Zhuang, W., Hillson, N.J., Keasling, J.D., Mukhopadhyay, A., 2017. A Cas9-based toolkit to
1177   program gene expression in Saccharomyces cerevisiae. Nucleic Acids Res. 45, 496–508.
1178   https://doi.org/10.1093/nar/gkw1023

1179   Renan, E.-C., Yonatan, S., M., C.S., B., I.J., Jue, W., J., M.C., Michael, S., 2015. Galactose
1180   metabolic genes in yeast respond to a ratio of galactose and glucose. Proc. Natl. Acad. Sci.
1181   112, 1636–1641. https://doi.org/10.1073/pnas.1418058112

1182   Reyes, L.H., Gomez, J.M., Kao, K.C., 2014. Improving carotenoids production in yeast via
1183   adaptive laboratory evolution. Metab. Eng. 21, 26–33.

1184 https://doi.org/https://doi.org/10.1016/j.ymben.2013.11.002

1185 Rodríguez-Porrata, B., Carmona-Gutierrez, D., Reisenbichler, A., Bauer, M., Lopez, G., Escoté,
1186 X., Mas, A., Madeo, F., Cordero-Otero, R., 2012. Sip18 hydrophilin prevents yeast cell
1187 death during desiccation stress. J. Appl. Microbiol. 112, 512–525.
1188 https://doi.org/10.1111/j.1365-2672.2011.05219.x

1189 Sánchez, B.J., Zhang, C., Nilsson, A., Lahtvee, P.-J., Kerkhoven, E.J., Nielsen, J., 2017.
1190 Improving the phenotype predictions of a yeast genome-scale metabolic model by
1191 incorporating enzymatic constraints. Mol. Syst. Biol. 13, 935.
1192 https://doi.org/10.15252/msb.20167411

1193 Santoyo-Garcia, J.H., Walls, L.E., Nowrouzi, B., Galindo-Rodriguez, G.R., Ochoa-Villareal, M.,
1194 Loake, G.J., Dimartino, S., Rios-Solis, L., 2022. In situ solid-liquid extraction enhances
1195 recovery of taxadiene from engineered Saccharomyces cerevisiae cell factories. Sep. Purif.
1196 Technol. 290. https://doi.org/https://doi.org/10.1016/j.seppur.2022.120880

1197 Santoyo-Garcia, J.H., Walls, L.E., Valdivia-Cabrera, M., Malci, K., Jonguitud-Borrego, N.,
1198 Halliday, K., Rios-Solis, L. 2023. The synergetic effect from the combination of different
1199 adsorption resins in batch and semi-continuous cultivations of *S. cerevisiae* cell factories to
1200 produce acetylated Taxanes precursors of the anticancer drug Taxol. bioRxiv.
1201 doi: https://doi.org/10.1101/2023.02.06.527354

1202 Sanz, A.B., García, R., Pavón-Vergés, M., Rodríguez-Peña, J.M., Arroyo, J., 2022. Control of
1203 gene expression via the yeast CWI pathway. Int. J. Mol. Sci.
1204 https://doi.org/10.3390/ijms23031791

1205 Sarrade-Loucheur, A., Ro, D.-K., Fauré, R., Remaud-Siméon, M., Truan, G., 2020. Synthetic
1206 derivatives of (+)-epi-α-bisabolol are formed by mammalian cytochromes P450 expressed in
1207 a yeast reconstituted pathway. ACS Synth. Biol. 9, 368–380.
1208 https://doi.org/10.1021/acssynbio.9b00399

1209 Schellenberger, J., Que, R., Fleming, R.M.T., Thiele, I., Orth, J.D., Feist, A.M., Zielinski, D.C.,
1210 Bordbar, A., Lewis, N.E., Rahmanian, S., Kang, J., Hyduke, D.R., Palsson, B.Ø., 2011.
1211 Quantitative prediction of cellular metabolism with constraint-based models: the COBRA
1212 Toolbox v2.0. Nat. Protoc. 6, 1290–1307. https://doi.org/10.1038/nprot.2011.308

1213 Signorell, A., Aho, K., Alfons, A., Anderegg, N., Aragon, T., Arachchige, C., Arppe, A., Baddeley,

1214   A., Barton, K., Bolker, B., Borchers, H.W., Caeiro, F., Champely, S., Chessel, D., Chhay, L.,

1215   Cooper, N., Cummins, C., Dewey, M., Doran, H.C., Dray, S., Dupont, C., Eddelbuettel, D.,

1216   Ekstrom, C., Elff, M., Enos, J., Farebrother, R.W., Fox, J., Francois, R., Friendly, M., Galili,

1217   T., Gamer, M., Gastwirth, J.L., Gegzna, V., Gel, Y.R., Graber, S., Gross, J., Grothendieck,

1218   G., Jr, F.E.H., Heiberger, R., Hoehle, M., Hoffmann, C.W., Hojsgaard, S., Hothorn, T.,

1219   Huerzeler, M., Hui, W.W., Hurd, P., Hyndman, R.J., Jackson, C., Kohl, M., Korpela, M.,

1220   Kuhn, M., Labes, D., Leisch, F., Lemon, J., Li, D., Maechler, M., Magnusson, A.,

1221   Mainwaring, B., Malter, D., Marsaglia, G., Marsaglia, J., Matei, A., Meyer, D., Miao, W.,

1222   Millo, G., Min, Y., Mitchell, D., Mueller, F., Naepflin, M., Navarro, D., Nilsson, H.,

1223   Nordhausen, K., Ogle, D., Ooi, H., Parsons, N., Pavoine, S., Plate, T., Prendergast, L.,

1224   Rapold, R., Revelle, W., Rinker, T., Ripley, B.D., Rodriguez, C., Russell, N., Sabbe, N.,

1225   Scherer, R., Seshan, V.E., Smithson, M., Snow, G., Soetaert, K., Stahel, W.A., Stephenson,

1226   A., Stevenson, M., Stubner, R., Templ, M., Lang, D.T., Therneau, T., Tille, Y., Torgo, L.,

1227   Trapletti, A., Ulrich, J., Ushey, K., VanDerWal, J., Venables, B., Verzani, J., Iglesias, P.J.V.,

1228   Warnes, G.R., Wellek, S., Wickham, H., Wilcox, R.R., Wolf, P., Wollschlaeger, D., Wood, J.,

1229   Wu, Y., Yee, T., Zeileis, A., 2022. DescTools: Tools for descriptive statistics.

1230   Simões, T., Mira, N.P., Fernandes, A.R., Sá-Correia, I., 2006. The SPI1 gene, encoding a

1231   glycosylphosphatidylinositol-anchored cell wall protein, plays a prominent role in the

1232   development of yeast resistance to lipophilic weak-acid food preservatives. Appl. Environ.

1233   Microbiol. 72, 7168–7175. https://doi.org/10.1128/AEM.01476-06

1234   Soneson, C., Love, M.I., Robinson, M.D., 2015. Differential analyses for RNA-seq: transcript-level

1235   estimates improve gene-level inferences [version 1; peer review: 2 approved].

1236   F1000Research 4. https://doi.org/10.12688/f1000research.7563.1

1237   Song, T.-Q., Ding, M.-Z., Zhai, F., Liu, D., Liu, H., Xiao, W.-H., Yuan, Y.-J., 2017. Engineering

1238   Saccharomyces cerevisiae for geranylgeraniol overproduction by combinatorial design. Sci.

1239   Rep. 7, 14991. https://doi.org/10.1038/s41598-017-15005-4

1240   Specht, S., Miller, S.B.M., Mogk, A., Bukau, B., 2011. Hsp42 is required for sequestration of

1241   protein aggregates into deposition sites in Saccharomyces cerevisiae. J. Cell Biol. 195,

1242   617–629. https://doi.org/10.1083/jcb.201106037

1243   Spitzner, A., Perzlmaier, A.F., Geillinger, K.E., Reihl, P., Stolz, J., 2008. The proline-dependent

1244   transcription factor Put3 regulates the expression of the riboflavin transporter MCH5 in

1245   Saccharomyces cerevisiae. Genetics 180, 2007–2017.

1246   https://doi.org/10.1534/genetics.108.094458

1247   Stephens, M., 2017. False discovery rates: a new deal. Biostatistics 18, 275–294.
1248   https://doi.org/10.1093/biostatistics/kxw041

1249   Thorpe, G.W., Fong, C.S., Alic, N., Higgins, V.J., Dawes, I.W., 2004. Cells have distinct
1250   mechanisms to maintain protection against different reactive oxygen species: oxidative-
1251   stress-response genes. Proc. Natl. Acad. Sci. U. S. A. 101, 6564–6569.
1252   https://doi.org/10.1073/pnas.0305888101

1253   Ulgen, E., Ozisik, O., Sezerman, O.U., 2019. pathfindR: An R package for comprehensive
1254   identification of enriched pathways in omics data through active subnetworks. Front. Genet.

1255   Vemuri, G.N., Eiteman, M.A., McEwen, J.E., Olsson, L., Nielsen, J., 2007. Increasing NADH
1256   oxidation reduces overflow metabolism in Saccharomyces cerevisiae. Proc. Natl. Acad. Sci.
1257   U. S. A. 104, 2402–2407. https://doi.org/10.1073/pnas.0607469104

1258   Walker, K., Croteau, R., 2000. Taxol biosynthesis: molecular cloning of a benzoyl-CoA:taxane
1259   2alpha-O-benzoyltransferase cDNA from taxus and functional expression in Escherichia
1260   coli. Proc. Natl. Acad. Sci. U. S. A. 97, 13591–13596.
1261   https://doi.org/10.1073/pnas.250491997

1262   Walls, L.E., Malcı, K., Nowrouzi, B., Li, R.A., D'Espaux, L., Wong, J., Dennis, J.A., Semião,
1263   A.J.C., Wallace, S., Martinez, J.L., Keasling, J.D., Rios-Solis, L., 2020. Optimizing the
1264   biosynthesis of oxygenated and acetylated Taxol precursors in Saccharomyces cerevisiae
1265   using advanced bioprocessing strategies. Biotechnol. Bioeng. 118, 279–293.
1266   https://doi.org/10.1002/bit.27569

1267   Walls, L.E., Martinez, J.L., Rios-Solis, L., 2022. Enhancing Saccharomyces cerevisiae taxane
1268   biosynthesis and overcoming nutritional stress-induced pseudohyphal growth.
1269   Microorganisms 10. https://doi.org/10.3390/microorganisms10010163

1270   Walls, L.E., Martinez, J.L., del Rio Chanona, E.A., Rios-Solis L. 2022. Definitive screening
1271   accelerates Taxol biosynthetic pathway optimization and scale up in *Saccharomyces*
1272   *cerevisiae* cell factories. Biotech. J. 17- 2100414. https://doi.org/10.1002/biot.202100414

1273   Wang, H., Marcišauskas, S., Sánchez, B.J., Domenzain, I., Hermansson, D., Agren, R., Nielsen,
1274   J., Kerkhoven, E.J., 2018. RAVEN 2.0: A versatile toolbox for metabolic network

1275   reconstruction and a case study on Streptomyces coelicolor. PLOS Comput. Biol. 14,
1276   e1006541.

1277 Yu, G., Wang, L.-G., Han, Y., He, Q.-Y., 2012. clusterProfiler: an R package for comparing
1278   biological themes among gene clusters. OMICS 16, 284–287.
1279   https://doi.org/10.1089/omi.2011.0118

1280 Zhang, T., Bu, P., Zeng, J., Vancura, A., 2017. Increased heme synthesis in yeast induces a
1281   metabolic switch from fermentation to respiration even under conditions of glucose
1282   repression. J. Biol. Chem. 292, 16942–16954. https://doi.org/10.1074/jbc.M117.790923

1283 Zuzuarregui, A., del Olmo, M., 2004. Expression of stress response genes in wine strains with
1284   different fermentative behavior. FEMS Yeast Res. 4, 699–710.
1285   https://doi.org/10.1016/j.femsyr.2004.01.008

1286

1287